

# Recent advances on characterization techniques for the composition-structure-property of solid electrolyte interphase

Hongyi Lu<sup>a, 1</sup>, Mangayarkarasi Nagarathinam<sup>b,c, 1</sup>, Yue Chen<sup>a,b, \*</sup>, Weijian Zhang<sup>a</sup>, Xi Chen<sup>d, \*</sup>, Jing Chen<sup>a</sup>, Jianming Tao<sup>a</sup>, Jiaxin Li<sup>a</sup>, Yingbin Lin<sup>a</sup>, Oleg V. Kolosov<sup>b,d, \*</sup>, Zhigao Huang<sup>a</sup>

a College of Physics and Energy, Fujian Normal University, Fujian Provincial Key Laboratory of Quantum Manipulation and New Energy Materials, Fuzhou 350117, China

b Physics Department, Lancaster University, Lancaster LA1 4YB, UK

c The Faraday Institution, Quad One, Harwell Science and Innovation Campus, Didcot OX11 0RA, UK

d State Key Lab of Heavy Oil Processing, College of Chemical Engineering, China University of Petroleum (East China), Qingdao 266580, China

**Keywords** Rechargeable battery, battery interface, solid electrolyte interphase, structure-property correlation, *in situ/operando*, real-time monitoring

**Abstract** The Solid Electrolyte Interphase (SEI) is a nanoscale thickness passivation layer that forms as a product of electrolyte decomposition through a combination of chemical and electrochemical reactions in the cell and evolves over time with charge/discharge cycling. The formation and stability of SEI directly determine the fundamental properties of the battery such as first coulombic efficiency (FCE), energy/power density, storage life, cycle life and safety. The dynamic nature of SEI along with the presence of spatially inhomogeneous organic and inorganic components in SEI encompassing crystalline, amorphous and polymeric nature distributed across the electrolyte to the electrolyte-electrode interface, highlights the need for advanced *in-situ/operando* techniques to understand the formation and structure of these materials in creating a stable interface in real-world operating conditions. This perspective discusses the recent developments in interface-sensitive *in-situ/operando* techniques, providing valuable insights and addressing the challenges of understanding the composition-structure-property of SEI and their correlations during the formation processes at spatio-temporal resolution across various length scales.

H.L.<sup>1</sup> and M.N.<sup>1</sup> contribute equally to this perspective.

Corresponding author: [yuechen@fjnu.edu.cn](mailto:yuechen@fjnu.edu.cn); [xi.chen@upc.edu.cn](mailto:xi.chen@upc.edu.cn); [o.kolosov@lancaster.ac.uk](mailto:o.kolosov@lancaster.ac.uk);

## List of abbreviations.

3D – Three-dimensional

ADF STEM – Annular dark-field imaging scanning transmission electron microscopy

AFM – Atomic force microscopy

APXPS – Ambient pressure X-ray photoelectron spectroscopy

Ag – Silver

Au – Gold

- 1 CEI – Cathode electrode interphase
- 2 C<sub>2</sub>H<sub>4</sub> – Ethylene
- 3 C<sub>1</sub>C<sub>6</sub>ImFSI – 1-hexyl-3-methylimidazolium bis(fluorosulfonyl)imide
- 4 C<sub>1</sub>C<sub>6</sub>ImTFSI – 1-hexyl-3-methylimidazolium (bis(trifluoromethanesulfonyl)imide)
- 5 CO – Carbon monoxide
- 6 CO<sub>2</sub> – Carbon dioxide
- 7 Cryo-TEM - Cryogenic transmission electron microscopy
- 8 Cu – Copper
- 9 CV – cyclic voltammogram
- 10 DEC – Diethyl carbonate
- 11 DMC – Dimethyl carbonate
- 12 DNP – Dynamic Nuclear Polarization
- 13 DS-PERS – Depth-sensitive plasmon-enhanced Raman spectroscopy
- 14 EC – Ethylene carbonate
- 15 EC-AFM – Electrochemical atomic force microscopy
- 16 EC-SFA – Electrochemical surface force apparatus
- 17 EDL – Electrical double layer
- 18 EELS – Electron energy loss spectroscopy
- 19 EEI – Electrolyte-electrode interface
- 20  $E_g$  – Energy gap
- 21 EMC – Ethyl methyl carbonate
- 22 EQCM – Electrochemical quartz crystal microbalance
- 23 EQCM-D – Electrochemical quartz crystal microbalance with dissipation
- 24 FEC – Fluoroethylene carbonate
- 25 FCE – First coulombic efficiency
- 26 FTIR – Fourier transform Infrared Spectroscopy
- 27 HAXPS – Hard X-ray photoelectron spectroscopy
- 28 HOPG – Highly oriented pyrolytic graphite
- 29 HOMO – Highest occupied molecular orbital
- 30 IL – Ionic liquid
- 31 Li – Lithium
- 32 LiClO<sub>4</sub> – Lithium perchlorate

- 1  $\text{LiCoO}_2$  – Lithium cobalt oxides
- 2  $\text{Li}_2\text{CO}_3$  – Lithium carbonate
- 3  $\text{LiF}$  – Lithium fluoride
- 4  $\text{LiTFSI}$  – Lithium bis(trifluoromethanesulfonyl)imide
- 5  $\text{Li}_x\text{MoO}_3$  – Lithium molybdate
- 6  $\text{Li}_2\text{O}$  – Lithium oxide
- 7  $\text{LiPF}_6$  – Lithium hexafluorophosphate
- 8 LUMO – Lowest unoccupied molecular orbital
- 9 MLLS – Multiple least squares fitting
- 10 NMR – Nuclear Magnetic Resonance
- 11 OXPS – operando X-ray photoelectron spectroscopy
- 12 PC – Propylene carbonate
- 13 QCM – Quartz crystal microbalance
- 14 SECM – Scanning electrochemical microscopy
- 15 SECCM – Scanning electrochemical cell microscopy
- 16 SEI – Solid electrolyte interface
- 17 SERS – surface-enhanced Raman spectroscopy
- 18 SFA - Surface force apparatus
- 19 SHINS – Shell-isolated nanoparticles
- 20 SXPS – Soft X-ray photoelectron spectroscopy
- 21 STEM – Scanning transmission electron microscopy
- 22 sXAS – soft X-ray absorption spectroscopy
- 23 TAG – Thermogravimetric analysis
- 24 TOF-SIMS – Time-of-Flight Secondary Ion Mass Spectrometry
- 25 UV – Ultraviolet
- 26 XPS – X-ray Photoelectron Spectroscopy
- 27

# 1. Introduction

## 1.1. What is Solid-Electrolyte Interphase (SEI)?

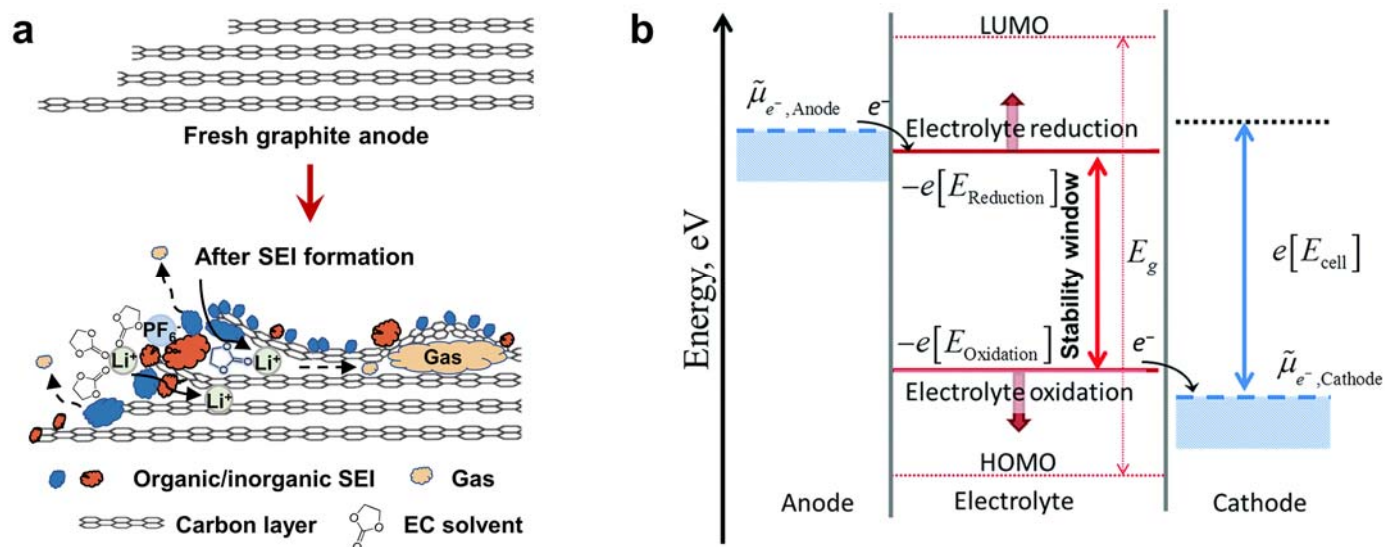


Figure 1 (a) Schematic of electrolyte decomposition and SEI formation in graphite anode. (b) The negative and positive voltage (potential) limits for the electrolyte stability, and the energy levels of the highest occupied molecular orbital (HOMO) and lowest unoccupied molecular orbital (LUMO), reproduced with permission. <sup>1</sup>Copyright 2018, RSC Publishing.

Solid-Electrolyte Interphase (SEI) is a passivation layer component that forms on the electrode surfaces of lithium/sodium-ion batteries during their initial electrochemical cycles and continues to evolve upon storage and charge/discharge cycling<sup>1-3</sup>. This SEI layer plays a critical role in stabilizing the interface between the electrode and electrolyte and in enhancing performance, longevity and safety of lithium/sodium-ion batteries. Ideally, SEI should be uniform, thin and chemically, electrochemically and mechanically stable. It is also vital for the lifespan and safety of lithium/sodium-ion batteries, acting as a protective barrier that stabilizes the interface between the electrode and the electrolyte<sup>4</sup>. By Hence an ideal SEI layer, not only prevents continuous electrolyte decomposition and limiting side reactions but also minimizes further growth of SEI. This in turn, reduces the SEI minimizes active material loss, and ensures efficient ion transport, maintains uniform alkali metal ion flux, suppresses dendrite growth and mechanical stress. Further, thereby preserving battery mitigates capacity fade and power fade thereby preserving the battery's performance capacity over time<sup>5</sup>. Additionally, it plays a crucial role in safety by mitigating risks such as reducing the risk of dendrite formation, thermal runaway, mitigating thermal runaway, and preventing the flammable exothermic gas generation that can lead to swelling or rupture<sup>6-8</sup>. Hence, it's very important to understand that, not only the basic components such as positive electrode, negative electrode, electrolyte and separator must be chemically, electrochemically and mechanically stable, but the newly formed SEI aA stable and well-formed SEI stability is also crucial is essential for enhancing battery durability and reliability, making its optimization a key focus of ongoing research<sup>9</sup>.

Taking the widely used graphite anode as an example (Figure 1a), the development of SEI layer is explained succinctly. The SEI layer originally derives from the sequential processes of "adsorption → decomposition → precipitation/growth" - of electrolyte components on the graphite electrode surface. This SEI layer then acts as a protective barrier that prevents further electrolyte reaction with the graphite edge and basal planes either by restricting electron tunnelling or by solvent diffusion<sup>3</sup>, which is increasingly significant toward designing novel secondary batteries, such as graphite-graphite dual-ion battery<sup>10</sup>. At the same time, the formation and growth of the SEI layer result in loss

of lithium inventory during repeated insertion/extraction of Li-ion as it consumes active lithium and electrolyte leading to capacity fading, increased battery resistance and low power density. However, it also plays a role in facilitating ion de-solvation and transportation between the graphite edge plane and electrolyte, preventing the co-intercalation of the strong coordinating solvent (such as EC) which often induces graphite delamination<sup>11</sup>. Therefore, the formation and stability of the SEI layer have a significant impact on the overall performance of the battery, including storage life, rate capability, cycle life and safety. Although the SEI is of nanoscale thickness and is insignificant compared to the overall size of Li-ion batteries, it plays a crucial role in its operation and functionality.

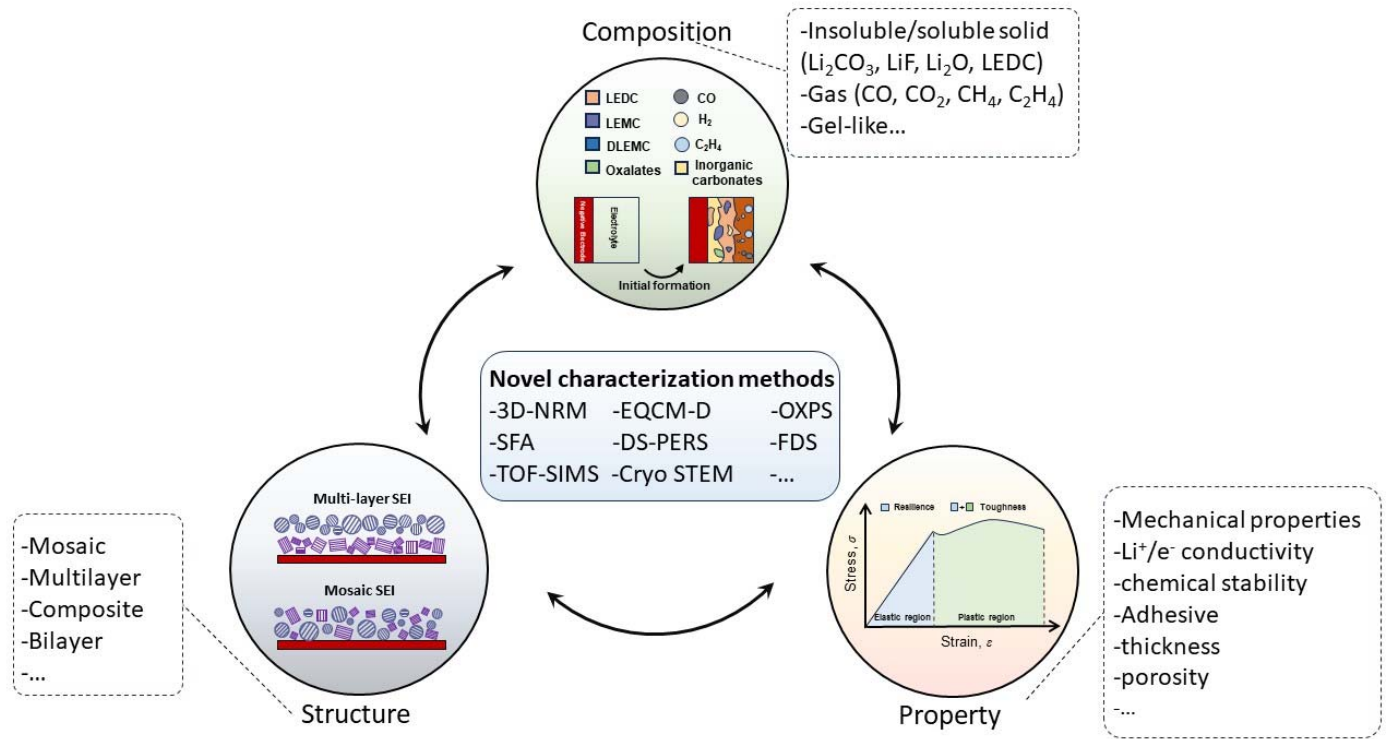
## **1.2. Fundamental perspectives on the formation of interfacial passivation layers**

The interfacial decomposition reactions of the electrolyte-electrode interface can be elucidated from the thermodynamic perspective considering electrolyte reactivity in terms of reduction and oxidation at high and low potentials, respectively. In the early stages, it has been postulated that the lowest unoccupied molecular orbital (LUMO) and highest occupied molecular orbital (HOMO) energy levels of the electrolyte dictate the thermodynamic stability of the battery electrolyte-electrode interface<sup>2</sup>. However, as shown in Figure 1b, a narrower electrochemical stable window compared to the energy gap ( $E_g$ ) between the LUMO and HOMO levels is often experimentally observed in the realistic battery electrolyte. Hubert et al further proposed the optimized electrode-electrolyte thermodynamic model based on redox potentials and Fermi level of the electron in solution to explain the electrolyte decomposition and SEI formation below the LUMO and above the HOMO energy levels. When the anode chemical potential ( $\tilde{\mu}_{e^-, Anode}$ ) is higher than the electrolyte reduction potential ( $-e[E_{reduction}]$ ), the electrons from the anode side can “jump” into the electrolyte, resulting in the reductive decomposition of the electrolyte. It is worth noting that a similar oxidation reaction can occur on the cathode side, resulting in the formation of SEI on the cathode surface, also commonly referred as cathode electrolyte interphase (CEI)<sup>1, 12</sup>.

Currently, commercial lithium-ion battery electrolytes comprise primarily cyclic (EC, FEC, PC, etc.) or linear carbonate solvents (DEC, EMC, DMC, etc.), lithium salts, and a minor quantity of functional additives. The reduction voltage ( $E_{reduction}$ ) and oxidation voltage ( $E_{oxidation}$ ) of commercial electrolyte is typically around 1.0 V and 4.7 V vs. Li<sup>+</sup>/Li, respectively. As a result, during the initial battery formation cycle, once the surface potential of the negative electrode material gradually decreases below 1.0 V, or that of the cathode side reaches 4.7 V, the reduction/oxidation and decomposition of electrolyte occurs and the insoluble products gradually accumulate on the electrode surface, ultimately forming the SEI membrane. By introducing an additive that can undergo reduction just before the electrolyte, the reduction of the liquid electrolyte can be prevented, and the integrity and robustness of the SEI can be improved.

To date, the interphases in lithium-ion batteries with liquid electrolytes at the anode/electrolyte and cathode/electrolyte surface are referred to as SEI and CEI respectively and the distinction between this nomenclature is unclear. However, this nomenclature is a misnomer, as it is also applied in emerging technologies like all-solid-state batteries. For those reasons, Amponsah et al. proposed a nomenclature for the interphase at anode/cathode with liquid electrolyte as liquid-electrolyte/anode interphase (LEAI) and liquid-electrolyte/cathode interphase (LECI)<sup>12</sup>. Although we agree with this and emphasize the need for clear naming, we are aware that it has to be discussed in detail to reach a consensus on nomenclature and it's out of the scope of this paper. Hence, in this paper, SEI refers to the interphase formed at the liquid electrolyte/anode in lithium-ion or lithium-metal batteries.

## **1.3. The composition-structure-property of SEI and their correlations**



1

2 Figure 2 Schematic of the composition, structure & property of SEI.

3 The chemical or electrochemical reactions involved in the formation mechanism of the SEI layer are  
 4 exceedingly complex due to the intricate composition of the electrolyte and driven by a diverse array  
 5 of chemical and electrochemical reactions influenced by factors such as the electrolyte, composition,  
 6 electrode surface chemistry includes the active sites and catalytic properties of the surface,  
 7 formation process parameters, and impurities such as water and acids<sup>3</sup>. To fully understand the  
 8 formation mechanism of SEI, one should start with the comprehensive characterization of SEI from  
 9 the perspective of compositions, nanostructures, as well as physical/chemical properties.

10 **1.3.1 Composition:**

11 The ultimate compositions of the SEI layer result from a complex interplay of various competing  
 12 reactions<sup>3, 13, 14</sup>. As shown in Figure 2, the decomposition products arising from electro-reduction  
 13 reactions encompass soluble, partly soluble or unstable deposits (lithium carbonate ( $\text{Li}_2\text{CO}_3$ ), lithium  
 14 oxalate ( $\text{Li}_2\text{C}_2\text{O}_4$ ) lithium alkoxides, lithium ethylene dicarbonate (LEDC) and lithium alkyl  
 15 carbonates), insoluble deposits (lithium fluoride, LiF), lithium oxide ( $\text{Li}_2\text{O}$ ), etc.) and gases like  $\text{H}_2$ ,  
 16  $\text{CO}$ ,  $\text{CO}_2$ ,  $\text{CH}_4$ , and  $\text{C}_2\text{H}_4$ . These gases can lead to gas evolution during the battery's cycling,  
 17 whereas soluble deposits may dissolve into the electrolyte itself. Only the insoluble deposits can  
 18 form various deposition structures on the negative electrode surface, ultimately constituting the SEI  
 19 layer<sup>3, 13, 14</sup>. Among them, although there still exists a controversy about the role of LiF in the SEI<sup>5</sup>,  
 20 LiF is the most commonly observed SEI component in various electrolyte-electrode combinations.  
 21 Considering the formation of similar degradation products in the interface films on both negative and  
 22 positive electrodes of conventional lithium-ion batteries, the existence of distinct acronyms SEI and  
 23 CEI rather than the anodic SEI and cathodic SEI and only reinstates the ambiguity in the  
 24 nomenclature as discussed earlier.

25 **1.3.2 Structure:**

26 SEI represents a region where the properties of two phases of interest, ie. electrode and electrolyte,  
 27 have undergone significant changes due to the chemical or electrochemical reaction between the

1 two phases, eventually resulting in the formation and growth of new products or phases with  
2 modified thickness. Therefore, SEI can be conceptualized as a three-dimensional contact of two  
3 phases having different physicochemical properties consisting of several phases and interfaces  
4 unlike, classical interfaces which are typically two dimensional<sup>15, 16</sup>. Researchers have identified  
5 various three-dimensional morphological arrangements of these decomposed products within the  
6 SEI, including mosaic, multilayer, and mixed structures<sup>17-19</sup>. As sketched in Figure 2, the mosaic  
7 structure of the SEI refers to a heterogeneous and patchy distribution of different components across  
8 the surface of the electrode. It's called "mosaic" because it appears as if different materials are  
9 arranged in irregular patterns, somewhat like a mosaic artwork<sup>17</sup>. While the multilayer structure of  
10 the SEI refers to the formation of distinct layers of different materials on the electrode surface<sup>18, 19</sup>.

11 **The two-layer SEI structure, consisting outside organic-rich component layer combined with an inner**  
12 **inorganic layer (LiF/LiCoO<sub>2</sub>), is generally considered as a stable and robust structure<sup>5, 20</sup>.** Additionally,  
13 the mixed structure of the SEI refers to a combination of different components, including inorganic  
14 and organic species, within the same layer or region<sup>19</sup>. Here, one should always bear in mind that  
15 the SEI is not a uniform and static layer, it undergoes changes and transformations during the cycling  
16 of the battery. Meanwhile, the variation in the compositions and structures – the arrangements of  
17 different components of the SEI can vary depending on factors like the type of electrode material,  
18 electrolyte composition, storage and cycling conditions.

### 19 **1.3.3 Properties:**

20 Apart from the components and nano-structures, researchers have also investigated the  
21 physical/chemical properties of the SEI layer using various analytical techniques<sup>3, 13, 14, 21</sup>. The  
22 physical properties of SEI refer to the thickness, porosity, mechanical strength and morphology,  
23 while the chemical properties ~~contain the component~~ include chemical composition, stoichiometry,  
24 electrochemical stability and ionic/electronic conductivity (ion/electron transfer characteristics). The  
25 SEI is typically a nanoscale thin layer, having a porous structure which can influence ion transport  
26 and diffusion within the layer. The mechanical properties of the SEI, such as its adhesion to the  
27 electrode surface, its ability to withstand the volume expansion, and the mechanical stress during  
28 continuous insertion/extraction of ions during charge/discharge cycles, are closely related to its  
29 chemical compositions and nanostructures. Thus, the chemical composition, stoichiometry, nano  
30 architecture and physicochemical properties of SEI are not fixed but evolve over cycling and are the  
31 determinant factors in the overall performance of batteries. The SEI should ideally allow the transport  
32 of lithium ions while preventing the passage of electrons. Managing electronic conductivity is  
33 essential to prevent continuous electron flow and maintain the electrochemical isolation of the  
34 electrodes. Comprehending the charge transfer dynamics and other physio-chemical properties of  
35 SEI is beneficial for the chemical stability of SEI. As instabilities in the SEI can lead to capacity  
36 fading, increased impedance, and safety concerns, researchers are continuously working on the  
37 development of advanced analytical techniques including spectroscopy, microscopy, and other  
38 surface science methods, to reveal the intrinsic nature of SEI in real time to provide deeper  
39 understanding between SEI and battery performance.

### 40 **1.4. Aims and scopes of this review**

41 Despite the crucial role of SEI in battery performance, the SEI layer has a thickness in the nanometre  
42 range, very sensitive and susceptible to change in environments and consists of a mixture of  
43 crystalline, nanocrystalline, amorphous and polymeric materials which are on the surface and buried  
44 underneath the surface. In addition to this, the structure and composition of the SEI evolve  
45 dynamically during charging and discharging. As there is a complex interplay between composition,  
46 structure and properties, understanding the physicochemical properties of this SEI presents a  
47 significant challenge. It is especially difficult to comprehend the effect of different phases from the

1 surface to the subsurface under dynamic conditions, which is essential for improving performance  
2 and safety. To date, there are a handful of reviews that highlight the state of development of *ex-situ*,  
3 *in situ* and *operando* studies to evaluate the battery interfaces<sup>22-24</sup>, a fundamental understanding of  
4 the composition-structure-properties correlation of SEI across various length scales by *in situ* or  
5 *operando* is rarely discussed except in modelling studies<sup>25</sup>. As our main objective is to obtain a vivid  
6 portrait of SEI to understand the complexity, this perspective highlights some recent literature on *ex-*  
7 *situ* and focuses mainly on recent advances *in situ* and *operando* techniques, the key findings,  
8 challenges and the importance of a multimodal approach to decouple the composition-structure-  
9 property of SEI and their correlations.

10 In Section 2, we will briefly discuss recent advances in *ex-situ* (or post-mortem) SEI characterization  
11 techniques, highlighting the significant advancements in enhancing surface sensitivity compared to  
12 the traditionally bulk-sensitive techniques, which have been instrumental in spatially resolving the  
13 nanoscale distribution of organic and inorganic components within the SEI layer. Section 3 delves  
14 into various recently developed *in situ* (or *operando*) techniques, providing that allow detailed  
15 examination-investigation of SEI characteristics/features, including nanostructures, nanomechanical  
16 properties, electrochemical activities, chemical compositions and so on. These innovative methods  
17 have unveiled new insights into the intrinsic properties, formation mechanisms, and impacts of the  
18 SEI on battery performance. Nevertheless, this article mainly explores the techniques that integrate  
19 both chemical and physical properties and offer a fresh viewpoint for examining the surface and  
20 sub-surface of the SEI at nanometer resolution. Finally, Section 4 summarizes our key perspectives  
21 on SEI characterization techniques and provides an outlook on their potential future research  
22 directions.

## 23 2. *Ex situ* characterization techniques

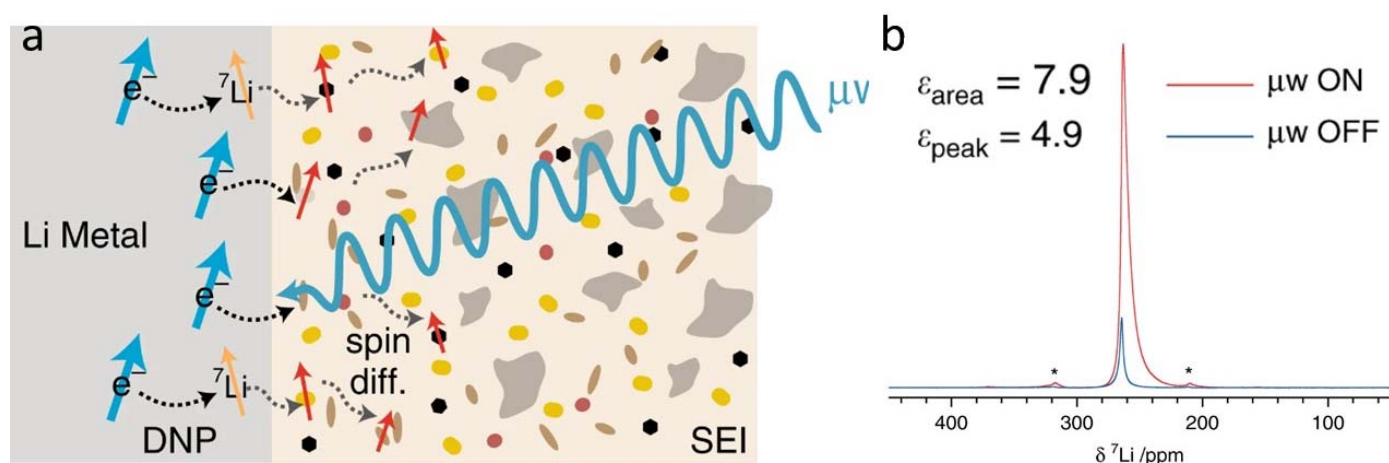
24 *Ex situ* or post-mortem analysis methods conventionally entail subjecting the electrode to initial  
25 cycling within a standardized battery cell unit and the sample for *ex situ* measurement undergoes a  
26 series of procedures, including washing and transfer, all conducted within the confines of a glovebox.  
27 This process carries with it the inherent risk of reactions occurring between the SEI and impurities  
28 present within the glovebox environment<sup>19</sup>. Such reactions may lead to the partial dissolution of the  
29 SEI and the transformation of metastable SEI compounds into more stable states. However, it is  
30 imperative to acknowledge that despite these challenges, *ex situ* characterization techniques have  
31 played a pivotal role in advancing our understanding of SEI films. The *ex-situ* or post-mortem, for  
32 example, various analytical techniques, including Infrared Spectroscopy (IR), X-ray Photoelectron  
33 Spectroscopy (XPS), Raman Spectroscopy, and Time-of-Flight Secondary Ion Mass Spectrometry  
34 (TOF-SIMS), Nuclear Magnetic Resonance (NMR) have been employed to elucidate the average  
35 chemical composition and molecular structure of the SEI layer and this has been discussed  
36 extensively in other Reviews<sup>24, 26-30</sup>.

37 This section discusses briefly on *ex-situ* methods where significant efforts have been made to  
38 enhance the surface sensitivity over the traditionally bulk-sensitive techniques and played a crucial  
39 role in spatially resolving the distribution of organic and inorganic components in the SEI layer at  
40 the nanoscale. Here, we highlight the substantial advancements made through the application of  
41 NMR spectroscopy in understanding the compositions and structures of SEI. The research team of  
42 Professor Clare Grey has developed room-temperature enhanced <sup>7</sup>Li, <sup>1</sup>H, and <sup>19</sup>F NMR spectra  
43 under magic angle spinning conditions by Overhauser Dynamic Nuclear Polarization (DNP). Here,  
44 the conduction electrons of lithium metal anode have been used as a free electron source to  
45 selectively amplify the signal in the order of magnitude at room temperature<sup>30</sup>. Although hyper  
46 polarization of lithium metal is not surface selective on the length scale, the subsequent spin  
47 diffusion from the hyperpolarized <sup>7</sup>Li metal anode could enhance only the SEI components which



1 are sufficiently close to interact with the conduction electron (Figure 3). This strategy has been used  
2 to reveal that LiF exists closer to the metal compared to other lithium-containing species such as  
3  $\text{Li}_2\text{CO}_3$  LEDC and lithium butylene dicarbonate (LBDC) and the thickness of SEI is thinner in 1.0 M  
4  $\text{LiPF}_6$  EC/DMC (LP30) with additive fluoroethylene carbonate (FEC) compared to electrolyte without  
5 additive. The outcomes of these studies have supported that the chemical composition and  
6 structural characteristics of the SEI are profoundly influenced by the choice of electrolyte system.  
7 Also, it supports the current understanding that SEI is impermeable to  $\text{PF}_6^-$ .

8 In this work, DNP has been utilized to study the buried/internal metal–diamagnetic solid–solid  
9 interfaces and hence, sheds light on the spatial distribution within the SEI interface in addition to the  
10 chemical composition of SEI. However, it is worth noticing that the NMR has yet to be realized in  
11 *operando* monitoring of SEI compositions and nano-structures in real battery conditions, and the  
12 physio-chemical properties of SEI have barely been revealed by NMR.



13  
14 Figure 3 (a) Pictorial representation of the effect of microwave application and the resultant hyperpolarization  
15 of Li metal (DNP, black dashed arrows) and spin diffusion in the heterogeneous mixed organic/inorganic SEI  
16 (gray dashed arrows). (b)  $^7\text{Li}$  NMR spectrum of microstructural lithium metal (sample A), with and without  
17 15.6 W of microwave irradiation at 395.29 GHz ( $\mu\text{w ON/OFF}$ ), recorded at 14.1045 T, 12.5 kHz MAS and a  
18 sample temperature of  $\sim 300$  K, using a Hahn echo pulse sequence showing the enhancement. Spinning  
19 sidebands are marked with an asterisk. Reproduced with permission.<sup>30</sup> Copyright 2020, Nature Publishing  
20 Group.

21 The employment of low-temperature conditions during sample preparation has proven beneficial in  
22 stabilizing sensitive battery materials and interfaces and highlights the importance of preserving the  
23 liquid and solid phases. This approach facilitates high-resolution characterization via cryogenic  
24 transmission electron microscopy (cryo-TEM, Figure 4), revealing amorphous nanoscale structures  
25 within diverse electrolyte systems, thus contributing valuable insights into the significance of SEI in  
26 different electrochemical contexts<sup>31, 32</sup>.

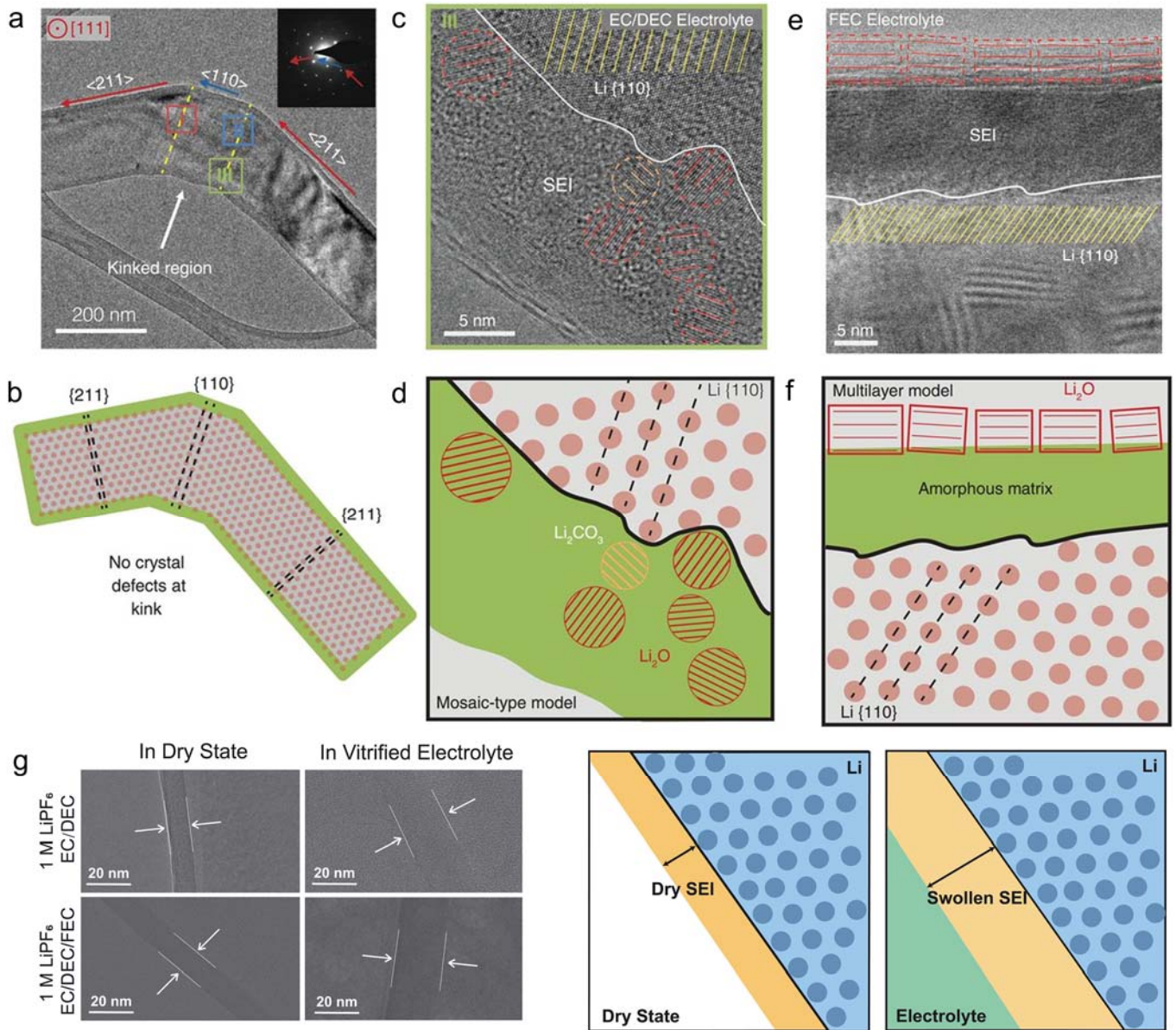


Figure 4 (a) TEM and (b) scheme of the single-crystalline nature of the kinked Li; (c) TEM and (d) scheme of the mosaic-type SEI layer; (e) TEM and (f) scheme of the multilayer-type SEI layer; (g) Comparison TEM and the scheme of the SEI in the dry and vitrified electrolyte. Reproduced with permission<sup>19, 31</sup>. Copyright 2017, AMERICAN ASSOCIATION FOR THE ADVANCEMENT OF SCIENCE. Copyright 2022, AMERICAN ASSOCIATION FOR THE ADVANCEMENT OF SCIENCE.

The first study of cryo-TEM from Cui et al. reveals the detailed nanostructure of the lithium metal dendritic growth within carbonate-based electrolytes, occurring primarily along  $\langle 111 \rangle$  (preferably),  $\langle 110 \rangle$ , or  $\langle 211 \rangle$  crystallographic directions, resulting in the formation of multi-faceted single-crystalline nanowires (Figures 4a, b)<sup>19</sup>. However, it is essential to note that this structural pattern is susceptible to environmental influences. The mosaic structure of the SEI layer in standard 1M NaPF<sub>6</sub> in EC: DEC electrolyte and layered structures in electrolyte with 10 % FEC additive (Figure 4c-f), and the structure change of the SEI when exposed to the electrolyte (Figure 4g) are displayed in Cryo-TEM. For example, when the SEI is not wetted, it primarily comprises alkyl carbonates originating from the carbonate-based electrolyte. The SEI exhibits swelling behaviour when exposed to wet conditions within the electrolyte, leading to an increased presence of carbonate-based organic molecules within the wetted SEI layer (Figure 4g)<sup>31</sup>. Further study indicates various components within the SEI assume differing roles. Amorphous organic constituents possess mechanical elasticity, allowing them to endure the volumetric expansion experienced during the charge and discharge processes of the negative electrode<sup>32, 33</sup>. In contrast, crystalline lithium

carbonate exhibits instability and susceptibility to decomposition upon interaction with lithium metal. Moreover, atomic-scale images from cryo-TEM studies by Bing et. al., confirm that  $\text{Li}_2\text{O}$  or the over-lithiated amorphous phase such as  $\text{LiO}_x$ ,  $\text{LiC}^+$  always buffer the  $\text{Li}_2\text{CO}_3$  from directly contacting the Li metal and also reveal the instability of lithium carbonate dispersed within the outer SEI which engages in continuous interactions with the electrolyte, leading to gas generation and, consequently, the formation of an evolving and porous SEI<sup>27, 33</sup>.

Interestingly, a recent study has provided additional insights into why FEC additives can improve the cycling life when running at the carbonate-based electrolyte<sup>28, 34</sup>. Within the mosaic-like SEI structure, there is an uneven distribution of inorganic nanoparticles, resulting in regions with a higher concentration of these nanoparticles exhibiting expedited lithium-ion conduction and faster lithium deintercalation rates. However, once the metallic lithium within these regions is exhausted, the remaining metallic lithium is unable to sustain a conductive pathway to the electrode, rendering it inactive, often referred to as "dead lithium." In contrast, within the layered SEI structure, the density of inorganic nanoparticles is relatively uniform, leading to comparable lithium-ion conduction rates across different regions<sup>28, 34</sup>. This uniformity facilitates a more even lithium deintercalation process throughout the SEI, thereby promoting a more homogeneous cycling behaviour.

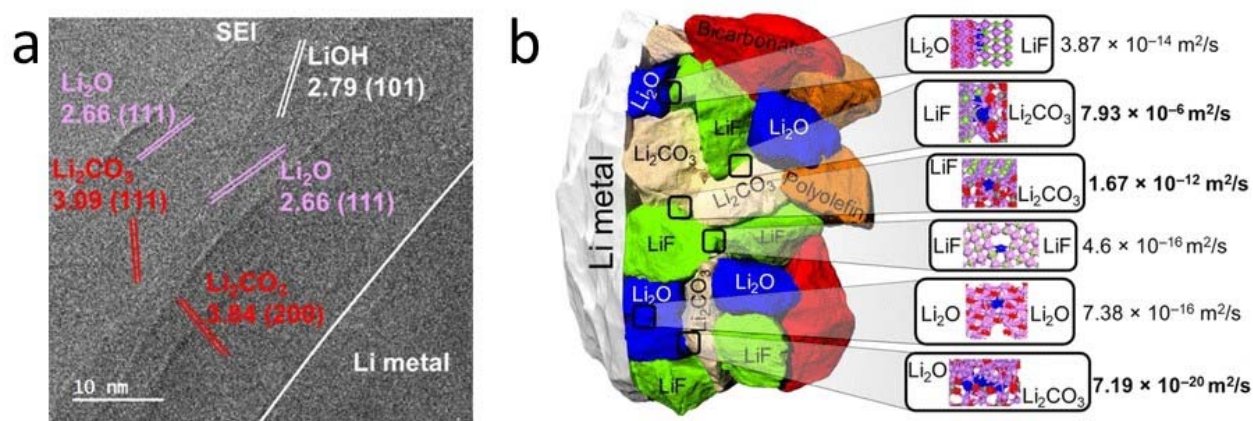


Figure 5 (a) Cryo-TEM image of the SEI layer formed on Li metal; (b) Pictorial representation of the nano structure of SEI identified from cryo-TEM and the diffusion coefficient in different grain boundaries using DFT simulations. Reproduced with permission<sup>35</sup> Copyright 2023, ACS Publications.

These cryo-TEM results have provided valuable information on the determination of SEI composition and structure in atomic scale/nanoscale resolution. However, the bulk inorganic components of SEI such as  $\text{Li}_2\text{CO}_3$ ,  $\text{Li}_2\text{O}$  and  $\text{LiF}$ , are rather poor  $\text{Li}^+$  conductors compared to the nanocrystalline phases of  $\text{Li}_2\text{O}$  and have moderate  $\text{Li}^+$  ion conductivities. It's also reported that  $\text{Li}^+$  ions are transported along grain boundaries between the different inorganic phases. This reveals that understanding the distribution of crystalline domains and the grain boundaries (GB) within the SEI is crucial for the uniform transport of lithium ions and underscores the importance of cryo-TEM in evaluating the failure modes of batteries. Hence, the impact of GBs in the SEI was investigated using cryo-HRTEM along with computational methods such as first principle calculations on the thermodynamic, kinetic, and electronic properties of the interface between the components<sup>35</sup>.

From cryo-HRTEM, a distinct SEI layer with an approximately 25-30 nm thickness composed of  $\text{Li}_2\text{O}$ ,  $\text{Li}_2\text{CO}_3$  and  $\text{LiOH}$  crystals with d-spacing 2.66, 3.09, 2.84, and 2.79 Å and lattices orientations along (110), (111) and (200) and (101) respectively are identified as grains (Figure 5a). Although, six grain boundaries were able to identify using cryo-TEM, only three stable configurations were found theoretically ( $\text{LiF}(111)/\text{Li}_2\text{CO}_3(200)$ ,  $\text{LiF}(111)/\text{Li}_2\text{CO}_3(002)$ , and  $\text{Li}_2\text{O}(111)/\text{Li}_2\text{CO}_3(111)$ ). Among these, the  $\text{LiF}(111)/\text{Li}_2\text{CO}_3(200)$  GB showed the highest rate of Li diffusion attributed to the favourable Li

1 multiatom coordination within the GB that facilitates the multiatom hopping mechanism, which is  
2 more advantageous compared to other diffusion mechanisms. Furthermore, analysis and  
3 comparison of the electronic structures of the GBs revealed that the  $\text{Li}_2\text{O}(111)/\text{Li}_2\text{CO}_3(111)$  GB is  
4 particularly prone to Li dendrite formation despite a relatively small diffusion coefficient. This  
5 combination of experiment and simulation suggests that the presence of this GB configuration may  
6 increase the likelihood of dendritic growth, which can pose safety risks and negatively impact the  
7 performance of Li-ion batteries. These results also reveal the importance of investigating the  
8 complex cooperative transport mechanisms of multi-components in the SEI layer compared to the  
9 single SEI components. Here, the advances in Cryo-TEM not only provided insight into the spatial  
10 distribution and the nanostructure of the SEI components, but it also been used to evaluate the  
11 transport properties of SEI. **Despite all these significances, the practical application and**  
12 **equitable/fair access is limited due to the high cost and technical challenges associated with**  
13 **conducting cryogenic experiments and vast/fast data collection.**

### 14 **3. Recent advances in novel *operando* characterization techniques**

15 Although the above post-mortem experiments effectively represent the formed SEI, they only reveal  
16 the static structure and composition information and there is a lack of insight into the intermediate  
17 states and the dynamic evolution of SEI during cycling. This limitation can lead to artefacts and  
18 encourages the researchers to focus on *in situ* or *operando* conditions for a more comprehensive  
19 understanding.

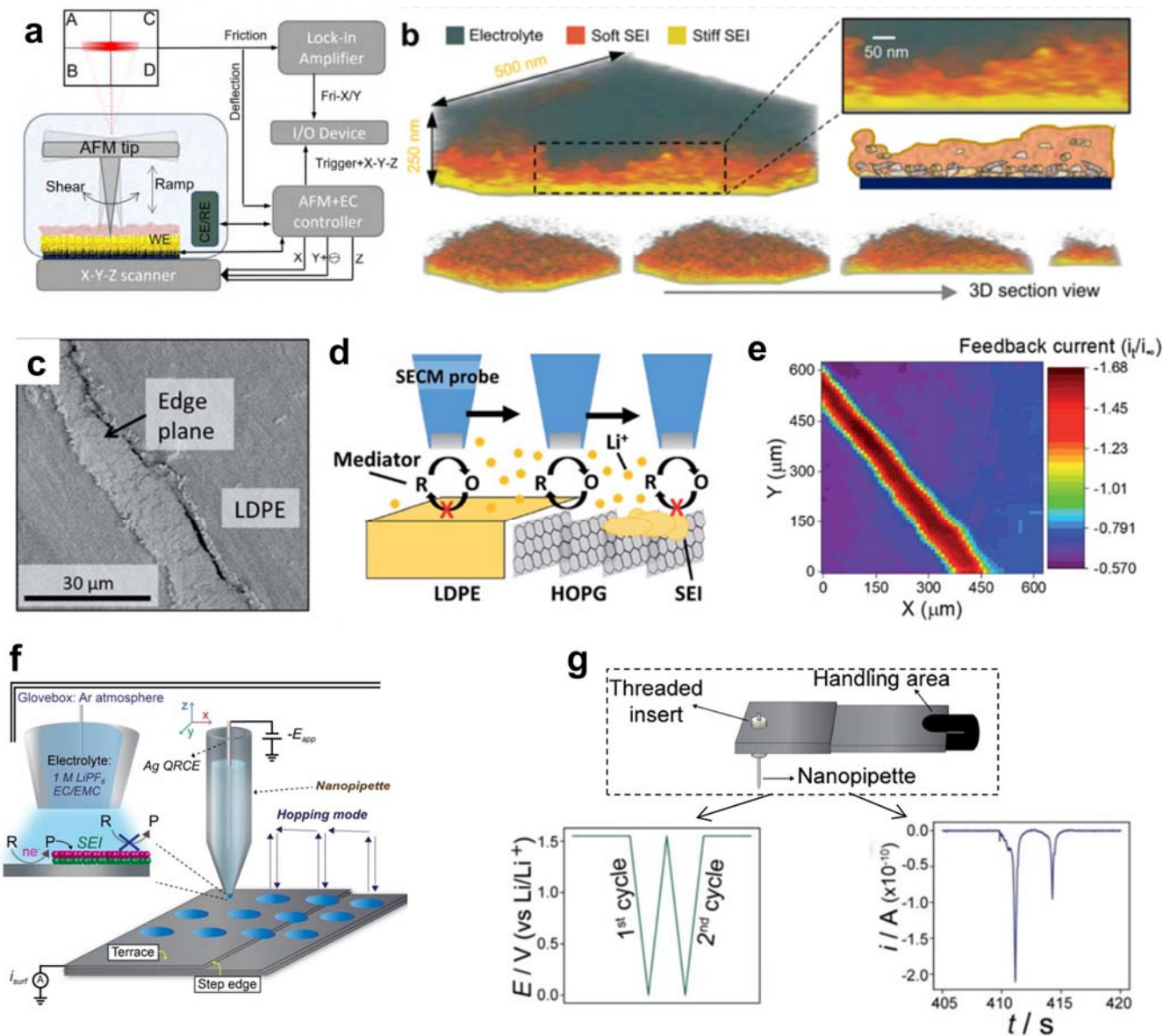
20 *Operando* SEI characterization techniques involve studying the SEI layer under realistic operating  
21 conditions, offering advantages over traditional *ex situ* (offline) characterization techniques when it  
22 comes to understanding battery performance. *Operando* techniques can capture the transient  
23 electrochemical reactions and directly link these processes to the electrochemical response of the  
24 battery which is often missed by *ex situ* techniques without altering the chemical and structural  
25 integrity of the interface regions. As mentioned above, more comprehensive reviews on the  
26 traditional characterization techniques that were used or modified as *operando* characterization  
27 techniques for SEI studies can be found in Refs<sup>13, 14, 36</sup>. In this article, we specifically focus on  
28 techniques and methodologies that amalgamate chemical or physical properties to provide a new  
29 perspective toward understanding the surface and sub-surface of SEI at nanometre resolution.  
30 Correlating the properties with the structural characteristics of the SEI from different perspectives is  
31 expected to offer unprecedented insights into its composition, structure, properties and  
32 electrochemical behaviour.

#### 33 **3.1 Advanced scanning probe microscopy**

34 Traditional *operando* electrochemical atomic force microscopy (EC-AFM) has been used to study  
35 SEI formation through the real-time monitoring of electrode surface topography with nano-scale  
36 resolution<sup>36</sup>. However, some key information about SEI, such as the mechanical moduli, fine  
37 nanoarchitecture, electrochemical activity and ionic transportation properties, are generally  
38 inaccessible by traditional EC-AFM techniques.

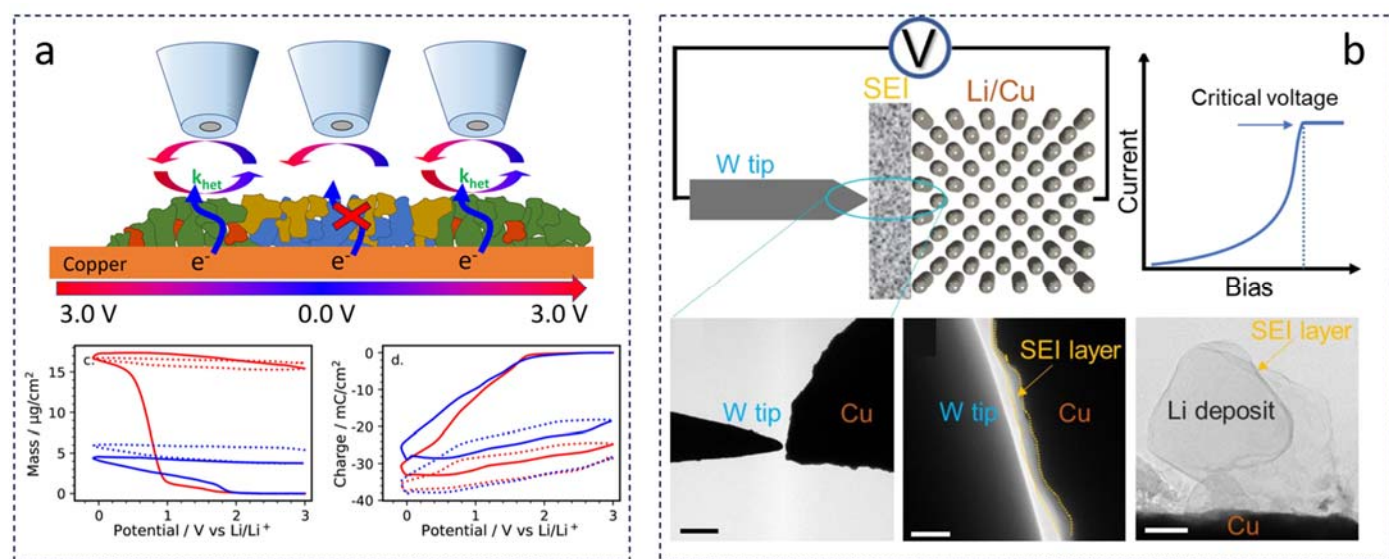
39 Recent studies focus specifically on obtaining these key SEI properties such as elasticity and  
40 viscosity to generate the nanoscale distribution of SEI organic/inorganic components, so-called SEI  
41 fine nanoarchitecture. For example, targeting the nanomechanical properties and nanostructure of  
42 SEI, Chen et al proposed the first three-dimensional nano-rheology microscopy<sup>11</sup> based on the shear  
43 modulation<sup>37</sup> mode EC-AFM (Figure 6a) which revealed the three-dimensional nanostructure of the  
44 SEI layer formed on graphite basal and edge planes in the real operational battery. Interestingly, the  
45 key information used to differentiate and reconstruct the three-dimensional structure of SEI is the  
46 viscosity, which was less noticed but had very distinct properties for the organic and inorganic parts

1 of SEI. Therefore, this new technique shows good spatial resolution and mechanical sensitivity  
 2 toward the different components inside the SEI layer (Figure 6b). Moreover, the electrical double  
 3 layer (EDL) structure is often considered to be a key part of initial SEI, in this work, the novel AFM-  
 4 based force distance spectroscopy<sup>38-41</sup> has also contributed significantly to the understanding of this  
 5 very initial EDL structure. Nevertheless, one should note that the contrast of force curves is still  
 6 under debate<sup>42</sup>, cautions need to be taken by researchers when studying the EDL structure by 3D  
 7 AFM force-distance curves. Although the correlations between EDL structure and SEI structures  
 8 need further systematic characterization studies, there is no doubt that nanostructures of SEI which  
 9 dominate their mechanical properties can be tuned by the EDL structures.



10  
 11 Figure 6 (a) Schematic of three-dimensional nano-rheology microscopy and (b) the observed three-  
 12 dimensional nanostructure of graphite edge plane SEI layer. (c) Scanning electron microscopy of an unused  
 13 region of HOPG edge for SECM measurements. (d) Illustration of SECM experimental setup and procedure  
 14 for SECM imaging and positioning. (e) SECM feedback image of the HOPG substrate. (f) Schematic of  
 15 SECCM operated in a hopping mode to study the formation of the solid-electrolyte interphase (SEI) at HOPG  
 16 electrodes. (g) The applied potential and the measured current as a function of time during a typical SECCM  
 17 experiment consisting of two voltammetric cycles at a pixel (spot on the surface). Reproduced with permission.  
 18 11, 43, 44. Copyright 2023, Nature Publishing Group. Copyright 2019, The Royal Society of Chemistry. Copyright  
 19 2021, John Wiley and Sons.

1 Apart from the nanostructure and nanomechanical properties of SEI, the electrochemical activity and charge transfer dynamics such as lithium-ion transportation kinetics and electron conductivity have been explored by scanning electrochemical microscopy (SECM)<sup>43, 45</sup> and scanning electrochemical cell microscopy (SECCM)<sup>44, 46, 47</sup> with a high spatial resolution. SECM and SECCM derive from AFM and are based on a similar piezo scanner system of AFM but with distinct tips or feedback signals. Zachary et al used Li<sup>+</sup>-sensitive probes to achieve *in situ* and localized tracking of Li<sup>+</sup> ions during the formation of the SEI and their subsequent intercalation processes. As shown in Figures 6c-e, by monitoring the potential-dependent reactivity of the graphite's edge planes, they investigated how the consumption of Li<sup>+</sup> ions at the interface led to competing reactions. Through cycling within the SEI formation potential range, their SECM measurements visualized both reversible ionic processes related to surface redox reactions and irreversible SEI formation, enabling the separation of charge-transfer steps at intricate battery interfaces. Prof. Patrick R. Unwin et al are the pioneers of introducing SECCM to study ion transportation in an electrochemical environment, including proton transportation through 2D materials<sup>48</sup> and lithium-ion diffusion through SEI layers<sup>44</sup>. As shown in the schematic diagram (Figure 6f) of SECCM proposed by Unwin et al, a mobile localized electrochemical probe operating in a hopping-mode protocol involved employing a single-barrel pipette. This pipette was loaded with electrolyte and an integrated Ag quasi-reference counter electrode. The procedure commenced by bringing the pipette in proximity to the sample surface. Upon establishing contact and forming a liquid meniscus, a cyclic voltammogram (CV) was recorded, as illustrated in Figure 6g. The most significant point of the SECCM set-up is to study the underlying local electrochemistry (spatially-resolved current-voltage relationship) of the SEI layer, which is essential for understanding the nanoscale lithium-ion transportation properties through the SEI layer and has not yet been revealed directly by other scanning probe microscopies.



25 Figure 7 (a) Schematic diagram of the combination of an SECM and electrochemical quartz crystal  
 26 microbalance for studying the SEI formation on Cu surface. (b) The combination of using TEM and AFM for  
 27 studying the SEI conductivity. Reproduced with permission. <sup>47, 49</sup> Copyright 2023, ACS Publications.  
 28 Copyright 2023, Nature Publishing Group.

29 The combination of SPM techniques and other *in situ* characterization techniques can provide an  
 30 additional degree of freedom for understanding SEI composition-structure-property correlations.  
 31 Krumov et al. visualized the SEI formation using SECM in feedback mode and showed that the  
 32 electronic conductivity of Cu decreases at 1.0 V indicating the incipient interphase formation and  
 33 kinetically limited SEI formation occurs at lower potentials<sup>47</sup> (Figure 7a). The observation of  
 34 significant current during lithium plating 100 μV, indicates that the SEI undergoes rupture in the  
 35 region where there is a development of lithium nucleation leading to positive feedback and tailing of

1 the distribution while regions that do not undergo lithium nucleation retain an intact SEI and  
2 maintains constant median. The subsequent lithium stripping studies reveal that the SEI is fully  
3 ruptured. The authors further validated the size and composition of the complex interfacial by  
4 complementary techniques such as *operando* electrochemical quartz crystal microbalance and *ex-*  
5 *situ* X-ray photoelectron spectroscopy (XPS). This observation of dynamically resolved SEI and the  
6 components by comprehending the key features such as mechanical and charge transfer properties  
7 provides solutions and insights to enhance the rational design of electrolytes and interphases in  
8 achieving better performance and safety<sup>47, 50</sup>. Xue et al. quantified the electrical properties of the  
9 SEI layer and battery performance by integrating *in situ* bias transmission electron microscopy (TEM)  
10 with scanning tunnelling microscopy (STM). As shown in Figure 7b, the measurement reveals that  
11 I-V characteristics of SEIs resemble certain electrical conductance rather than electrical insulators  
12 as conceived in other studies. This study also confirmed that the SEI with a higher rate differential  
13 conductance tends to exhibit a greater thickness and more complex topographic features leading to  
14 an inferior electrochemical performance<sup>49</sup>.

15 Future advancements in electrochemical SPM for SEI studies must emphasize the importance of  
16 high-speed image capturing capability, which is crucial for observing the sub-second-scale dynamic  
17 evolution of SEI during electrochemical processes, providing valuable insights into its formation  
18 mechanisms and a more precise understanding of its morphological and mechanical properties.  
19 Under high scanning speed, the ability to maintain low-force interactions, which minimizes tip-  
20 induced damage or alteration of the delicate SEI layer, becoming more an important factor. Moreover,  
21 real-time *operando* capabilities that can capture SEI evolution under varying cycling conditions,  
22 temperatures, and chemistries are essential to bridge the gap between fundamental insights and  
23 practical battery performance optimization. By improving both these aspects, SPM-based  
24 techniques can enable more reliable and detailed investigations of the SEI, advancing our  
25 understanding of its role in battery performance and stability.

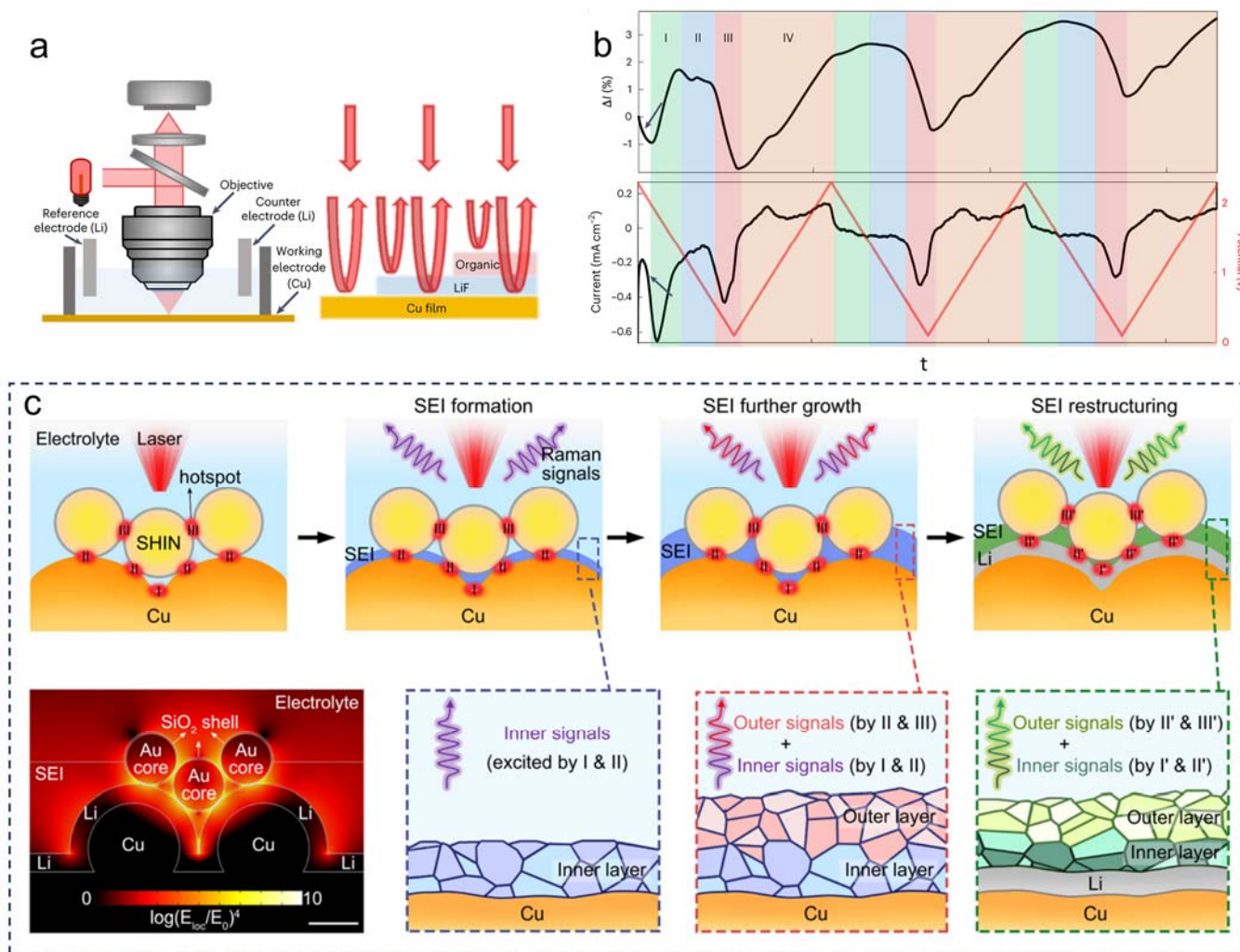
### 26 **3.2 Optical methods**

27 Optical characterization methods combined with electrochemical measurements offer several  
28 advantages, such as non-destructive, easy implementation, and multi-modal capabilities, when  
29 studying the electrode-electrolyte interface in batteries. Many optical methods<sup>51-57</sup> including  
30 Raman/FTIR/UV-visible light spectroscopy, ellipsometry, and embedded optical fibre sensor, have  
31 been used to study the battery electrode-electrolyte interface and provided quantitative information  
32 about the electrode phase and SEI composition changes, as well as the charge storage mechanisms.

33 Visible light has the advantage of studying the optical band gap changed by lithium-ion intercalation,  
34 and therefore *operando* optical microscopy has been used to study the lithiation/de-lithiation induced  
35 electronic structure changes of electrode materials, such graphite anode<sup>52</sup>, LiCoO<sub>2</sub> cathode<sup>54, 56</sup>  
36 Li<sub>4</sub>Ti<sub>5</sub>O<sub>12</sub><sup>58</sup> and Nb<sub>14</sub>W<sub>3</sub>O<sub>44</sub> anode<sup>53</sup>. Although the thickness of SEI is at a range of a few to hundred  
37 nano metres that is typically out of the resolution limit of visible optical methods, optical microscopy  
38 with reflection interference geometry has been introduced to reveal the evolution of SEI formed on  
39 electrode surfaces. As shown in Figure 8a, Shan et al proposed a non-intrusive, real-time reflection  
40 interference microscope to capture the dynamic processes of formation and evolution of SEI with  
41 exceptional sensitivity<sup>55</sup>. The key optical properties used to differentiate the SEI component are the  
42 reflective index of different SEI components and their thickness. By recording the reflectance of the  
43 Cu electrode-electrolyte interface (Figure 8b), they observed the emergence of a lasting inner  
44 inorganic layer primarily composed of LiF, a brief establishment of an electrochemically charged  
45 double layer at the interface, and the subsequent appearance of a temporary outer layer rich in  
46 organic compounds. Moreover, it is worth noting that, visible light spectroscopy techniques can often  
47 be combined with other characterization methods, such as electrochemical impedance

1 measurements, to provide a more comprehensive understanding of SEI formation and interface  
 2 dielectric properties<sup>59</sup>. This multi-modal approach allows researchers to correlate the optical and  
 3 dielectric properties of SEI with the overall electrochemical behaviour of the electrodes.

4 Raman and FTIR techniques can further provide the chemical composition information of SEI with  
 5 molecule structure resolution<sup>60</sup>. The limited sensitivity of vibrational spectroscopy, in terms of the  
 6 requisite analyte concentration, renders the distinction of complex SEI species from the vibrational  
 7 spectra of the electrolyte virtually unattainable. For example, in the context of *in situ* infrared  
 8 research, it has been discerned that the spectral response is primarily dictated by changes in lithium  
 9 coordination within the electrolyte. Notably, signals stemming from the final SEI species are  
 10 essentially absent<sup>22, 61</sup>. Therefore, to access information predominantly from the nanoscale SEI  
 11 structure by employing infrared and visible light, it is theoretically imperative to transcend the  
 12 diffraction constraints<sup>51</sup>. Recently, a novel depth-sensitive plasmon-enhanced Raman spectroscopy  
 13 (DS-PERS)<sup>51</sup> facilitates the non-destructive and *in situ* analysis of the nanostructure and chemical  
 14 properties of the SEI with single molecule detection sensitive and sub-nanometre scale spatial  
 15 resolution. This is achieved through the cooperative amplification of localized surface plasmons  
 16 utilizing nanostructured copper, shell-isolated gold nanoparticles, and lithium deposits positioned at  
 17 varying depths (Figure 8c). The proposed DS-PERS investigation yields detailed molecular-level  
 18 insights that uncover the significant impact of lithium on altering the formation of the SEI, shedding  
 19 light on the functions of SEI in controlling the de-solvation of lithium ions and the subsequent  
 20 deposition of lithium at interfaces associated with the SEI.



21  
 22 Figure 8 (a) Schematic diagram of using RIM to image the SEI formation dynamics. (b) The optical reflection  
 23 signal (RIM signal) during the first three CV cycles. (c) Schematics of the DS-PERS that enable detection of

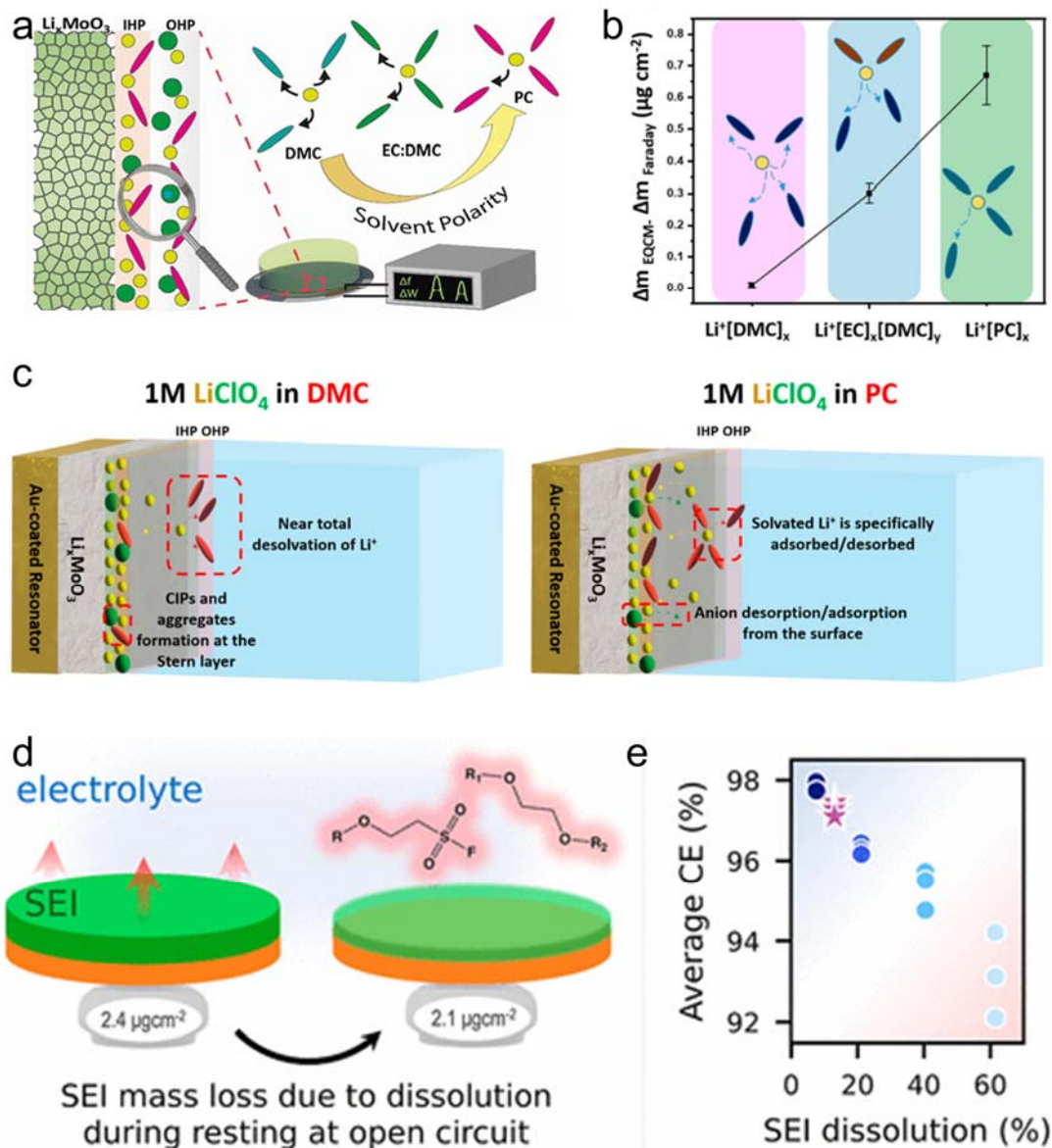


1 the signals from different depths in the SEI. The plasmonic structure of nanostructured Cu, SHINs and  
2 deposited Li generates a strong electromagnetic field to enhance the Raman signals from SEIs. Reproduced  
3 with permission.<sup>51, 55</sup> Copyright 2023, Nature Publishing Group. Copyright 2023, Nature Publishing Group.

4 In summary, these novel optical methods have been versatile and powerful toolkits for studying SEI  
5 formation in batteries, providing insights into dynamic processes, chemical composition, and  
6 structural changes, as well as contributing to a deeper understanding of battery performance and  
7 degradation mechanisms. The surface-enhanced Raman spectroscopy (SERS) techniques<sup>57, 62, 63,</sup>  
8 were also employed to investigate the stepwise SEI formation process on Au substrates immersed  
9 in a model electrolyte comprising LiClO<sub>4</sub> dissolved in EC solvent<sup>63</sup>. This approach facilitated the  
10 differentiation of effects associated with electrode/electrolyte bilayer charging, electrode adsorption  
11 polarization (the Stark effect), and SEI dissolution. The principal products formed at ca. 2 V vs. Li<sup>+</sup>/Li  
12 were identified as Li<sub>2</sub>CO<sub>3</sub> and Li<sub>2</sub>O. Furthermore, under the catalytic influence of the Au interface,  
13 the reduction of EC was determined to be a two-electron process, yielding Li<sub>2</sub>CO<sub>3</sub> and C<sub>2</sub>H<sub>4</sub> gas.  
14 Notably, CO<sub>2</sub> plays a pivotal role in both chemical and electrochemical reduction pathways. The  
15 authors emphasized the significance of gas diffusion at the interface and the potential presence of  
16 contaminants during sample preparation, both of which could introduce misleading factors into the  
17 final test results within the context of interface processes<sup>63</sup>. In the future, the integration of high-  
18 resolution techniques, such as tip-enhanced Raman spectroscopy, could enable nanoscale  
19 chemical mapping of SEI components with unprecedented detail. Meanwhile, the development of  
20 advanced optical probes and tailored substrates that enhance sensitivity to weakly scattering  
21 species in the SEI can reveal subtle chemical changes. Lastly, leveraging machine learning  
22 algorithms to analyze large spectroscopy datasets could provide deeper insights into the complex  
23 correlations between SEI composition, structure, and battery performance.

### 24 **3.3 Electrochemical quartz crystal microbalance (EQCM)**

25 Electrochemical quartz crystal microbalance, often abbreviated as "EQCM", is a specialized  
26 analytical instrument used in electrochemistry and materials science. The basic function of a quartz  
27 crystal microbalance is to measure changes in the resonance frequency of a quartz crystal electrode  
28 as a result of mass changes occurring on its surface. When used in an electrochemical context, the  
29 EQCM can provide valuable information about processes such as electrodeposition, corrosion, and  
30 the formation of thin films or coatings. Recently, EQCM with the added ability to monitor changes in  
31 dissipation during electrochemical processes (EQCM-D)<sup>64, 65</sup> has driven much research attention.  
32 EQCM-D enables measuring changes in crystal oscillation energy loss or damping during  
33 electrochemical processes<sup>66</sup>, providing information about mass changes (frequency) and  
34 viscoelastic properties (dissipation) of the SEI layer as it forms and evolves. This information can be  
35 used to understand the SEI layer's growth rate, thickness, and viscoelastic properties, as well as  
36 the mechanical properties and stability of the SEI.



1

2 Figure 9. (a) Schematic illustration of studying solvation structure inside EDL by EQCM. (b) The tendency of  
 3 the difference between both masses ( $\Delta m_{\text{EQCM}} - \Delta m_{\text{Faraday}}$ ) following the binding energy of solvated  $\text{Li}^+$  species  
 4 in each solvent. (c) Schematic illustration of the EDL structure evolution related to solvent polarity. (d)  
 5 Schematic diagram of SEI dissolution revealed by the mass changes recorded by EQCM. (e) The relation  
 6 between the coulombic efficiency and the mass percentage of SEI dissolution. Reproduced with permission.  
 7 <sup>67, 68</sup>. Copyright 2023, ACS Publications. Copyright 2022, ACS Publications.

8 Since the initial SEI formation is closely related to the electrical double layer (EDL) structure, an  
 9 emerging novel application of EQCM in battery interface research is the deciphering of the EDL  
 10 structures, observation of EDL charging and initial SEI formation<sup>68-70</sup>. As shown in Figure 9a, Ozlem  
 11 et al. conducted an EQCM investigation into the impact of different combinations of solvents and  
 12 salts, each varying in dipole moment and size/weight, on the structural characteristics of the EDL  
 13 forming at the electrolyte-electrode interface (EEI) of  $\text{Li}_x\text{MoO}_3$ . The research highlights the  
 14 substantial involvement of solvated lithium ions and anions in charge compensation at EEI. By  
 15 altering the solvent type, and distinguishing between cyclic and noncyclic solvents, they provide  
 16 compelling experimental evidence for the direct correlation between ion solvation and solvent  
 17 polarity (Figure 9b). Figure 9c illustrates that EQCM-D detected an anionic response characterized  
 18 by (electro)adsorption/desorption in electrolytes containing highly polar solvents like PC or EC: DMC  
 19 mixtures. This is in contrast to less polar solvents like DMC, where there is a greater possibility of

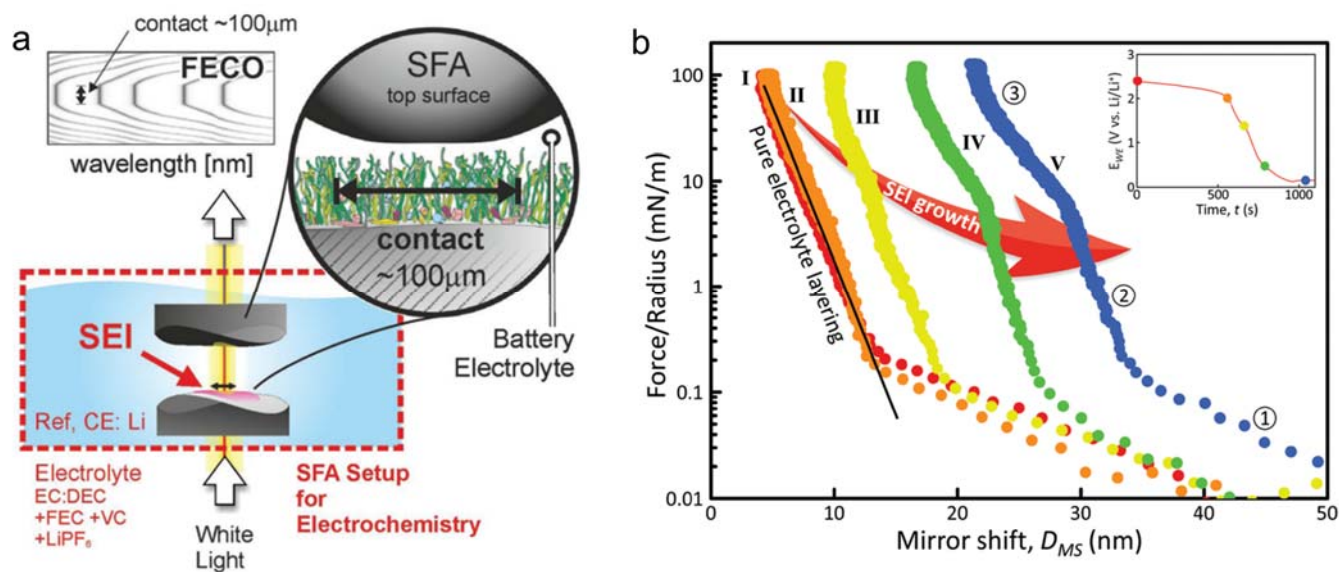
1 CIP formation and aggregate formation. This observation using EQCM-D signifies the profound  
2 influence of solvent choice on EDL behaviour and later formed SEI. This further revealed that, by  
3 utilizing EQCM, the *in situ/operando* chemical stability of SEI can be quantified by evaluating the  
4 SEI dissolution and growth at  $\text{ng}/\text{cm}^2$  scale. It has been demonstrated that over half of the SEI mass  
5 is lost during battery rest<sup>71</sup>. Further, by comparing the EQCM results with the coulometric  
6 experiments (Figures 9d and 9e), Sayawong et al corroborated that SEI dissolution is the major  
7 contributor toward SEI evolutions and established a correlation among solubility, passivity and  
8 cyclability, therefore, they added that physical and chemical properties of SEI plays a major role in  
9 minimizing the capacity loss<sup>67</sup>. Due to the limited volume expansion of graphite-based anode during  
10 cycling, this dissolution of SEI is not that detrimental compared to lithium metal batteries which  
11 undergo high volume expansion<sup>67, 72, 73</sup>.

12 Although EQCM can provide direct results from the obtained molecular mass, qualitative and  
13 quantitative characterization of EQCM response changes during SEI formation and automatically  
14 generate atomistic models of SEI components that are compatible with EQCM data remain  
15 challenging. ALC-EQCM – a software developed for post-processing EQCM data attempts to link  
16 EQCM data with simulation capabilities<sup>74</sup>. The post-process of EQCM data using ALC-EQCM may  
17 offer an effective strategy to explore reaction configurations only compatible with experiments and  
18 support the research of complex reactions that generate unexplored SEI components in a new  
19 electrolyte system. In the future, integration of EQCM with other complementary techniques, such  
20 as spectroscopic or electrochemical impedance methods, could provide a more holistic  
21 understanding of the dynamic interplay between SEI mass changes, composition, and  
22 electrochemical activity. Developing *operando* EQCM setups that can operate under realistic battery  
23 conditions, including high current densities and extreme temperatures, will be essential for studying  
24 SEI behaviours in practical environments. Lastly, but most importantly, innovations in interpreting  
25 EQCM data, such as advanced modelling techniques, could improve the resolution of solvent, ion,  
26 and other species' contributions to SEI dynamics, offering deeper insights into its formation  
27 mechanisms and long-term stability.

### 28 **3.4 Surface force apparatus**

29 Electrochemical surface force apparatus (EC-SFA) is a novel SEI characterization technique that  
30 combines the principles of a surface force apparatus with electrochemical techniques, specifically  
31 good at studying the molecular interaction forces on the battery interface<sup>75, 76</sup>. The proposed  
32 methodology has served as a unique and valuable new tool for analysing and ultimately tuning the  
33 mechanical properties of SEI layers. As shown in Figure 10a, it consists of two parallel surfaces or  
34 mica sheets that can be brought into proximity and separated, allowing for precise measurements  
35 of forces (e.g., van der Waals, electrostatic, capillary) as a function of the distance between the  
36 surfaces. In an EC-SFA setup, the SFA apparatus is modified to include an electrochemical cell or  
37 chamber. This allows researchers to control the electrochemical environment, including the  
38 composition of the electrolyte solution and applied potential, while simultaneously measuring forces  
39 between the surfaces. Renner et al used *in situ* SFA to observe the surface force-distance curves  
40 on a gold working electrode surface during the SEI formation cycles<sup>76</sup>. A clear signature for a new  
41 compressible film can be recognized in the force-distance characteristic upon electrode discharge  
42 (Figure 10b), and the increased force slope was observed at the low discharge voltage region,  
43 indicating a compressible nature of SEI. Their SFA results demonstrate that SEIs are to a large  
44 volume fraction polymeric and potentially flexible. Therefore, tuning of polymeric structures in the  
45 SEI layer will hence provide a viable strategy for optimizing performance during large volume  
46 expansion and contraction cycles. Future developments should focus on integrating SFA with  
47 complementary spectroscopic techniques, which could reveal the relationship between SEI  
48 composition and its interfacial mechanics. Developing more sophisticated models to interpret SFA

1 data in the context of complex, dynamic SEI environments will further strengthen its role in  
2 advancing our understanding of SEI behaviour.

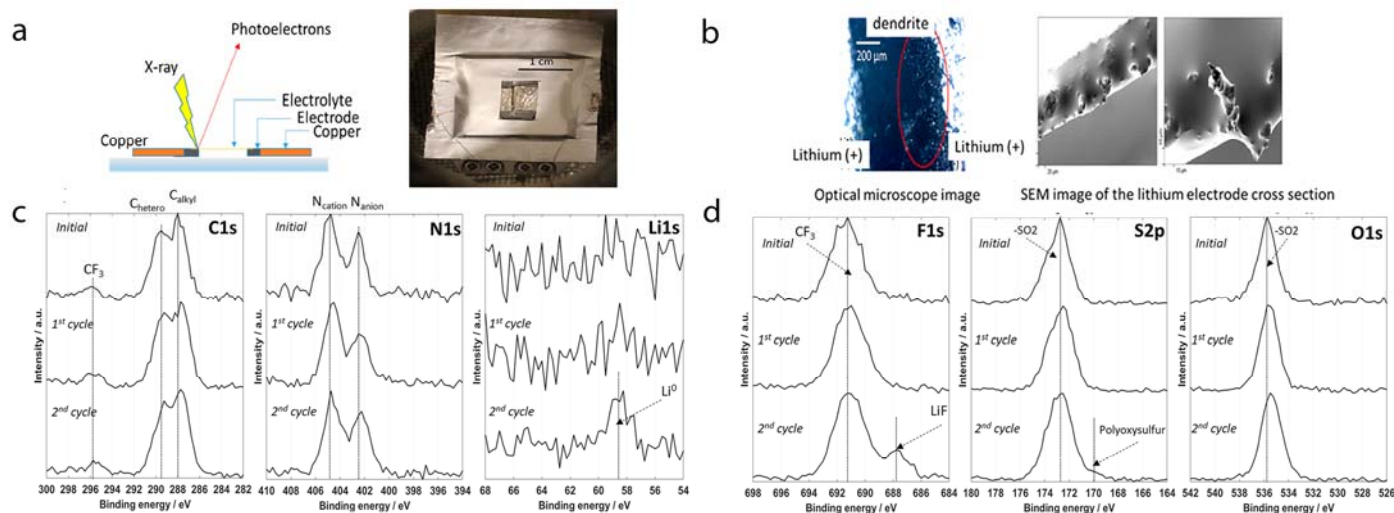


3  
4 Figure 10 (a) Experimental setup of the electrochemical surface forces apparatus (SFA), modified for lithium-  
5 ion battery testing (battery-SFA). (b) Force run curves on the SEI on gold-coated mica, taken on different  
6 depths of discharge, indicated by voltage-time curve (inset). Reproduced with permission.<sup>75, 76</sup> . Copyright  
7 2019, John Wiley and Sons. Copyright 2016, Nature Publishing Group.

### 8 **3.5 Operando XPS**

9 It's well known that, XPS is an indispensable technique to determine the qualitative and quantitative  
10 chemical composition, oxidation states and chemical environment of the probed elements in SEI  
11 and has opened new avenues to understand the redox processes and surface reactions that occur  
12 at the battery interfaces under post-mortem conditions<sup>22, 77</sup>. Since, high-energy X-ray beams are  
13 expected to damage the nanometer-thick SEI, hard and soft X-ray photoelectron spectroscopy  
14 (HAXPS and SXPS) have been used to understand the interface of solid-electrolyte interphase.  
15 However, the limitations such as ultra-high vacuum environment (UHV), shallow depth analysis (~  
16 5 nm) and the lateral resolution imposed by the X-ray beam of conventional XPS hindered their  
17 ability to study the chemical composition, charge transfer and the nature of chemical bonds of SEI  
18 in real battery environments. Therefore, to fully understand the complex solid-liquid interfaces in a  
19 battery, measurements at high pressure or ultra-low vacuum are required to analyse the interfaces,  
20 including the liquid phase.

21 The major challenge experienced with this technique is the scattering of photoelectrons before  
22 detection. To maximise the gain of photoelectrons under the desired pressure in the chamber, the  
23 aperture and the beam spot were kept at the same size<sup>78</sup>. To measure the nanometer thickness SEI,  
24 ambient pressure XPS (APXPS) measurement was developed, in which the electrodes are  
25 immersed in the electrolyte and then slowly retracted from the beaker to create a thin liquid meniscus.  
26 These techniques are becoming increasingly common and various electrolytes have been  
27 investigated using static droplets and liquid jet setups. These studies show that APXPS not only  
28 provides information on oxidation state and surface layer formation but also offers unique  
29 capabilities to provide information on electrode potential differences<sup>79, 80</sup>.



1

2 Figure 11 (a) Design of planar-like cell and the OXPS pouch cell (b) Optical and SEM images recorded after  
 3 polarization, demonstrating the formation of lithium dendrites with needle-like shape. (c-d) C 1s, N 1s, Li 1s,  
 4 F 1s, S 2p, and O 1s were recorded at the interface Li/C<sub>1</sub>C<sub>6</sub>ImTFSI-LiTFSI during the polarization at the  
 5 current density of 200  $\mu\text{A cm}^{-2}$  in the OXPS cell. The spectra were recorded after GEIS measurement.  
 6 Reproduced with permission.<sup>81</sup>. Copyright 2021, ACS Publications.

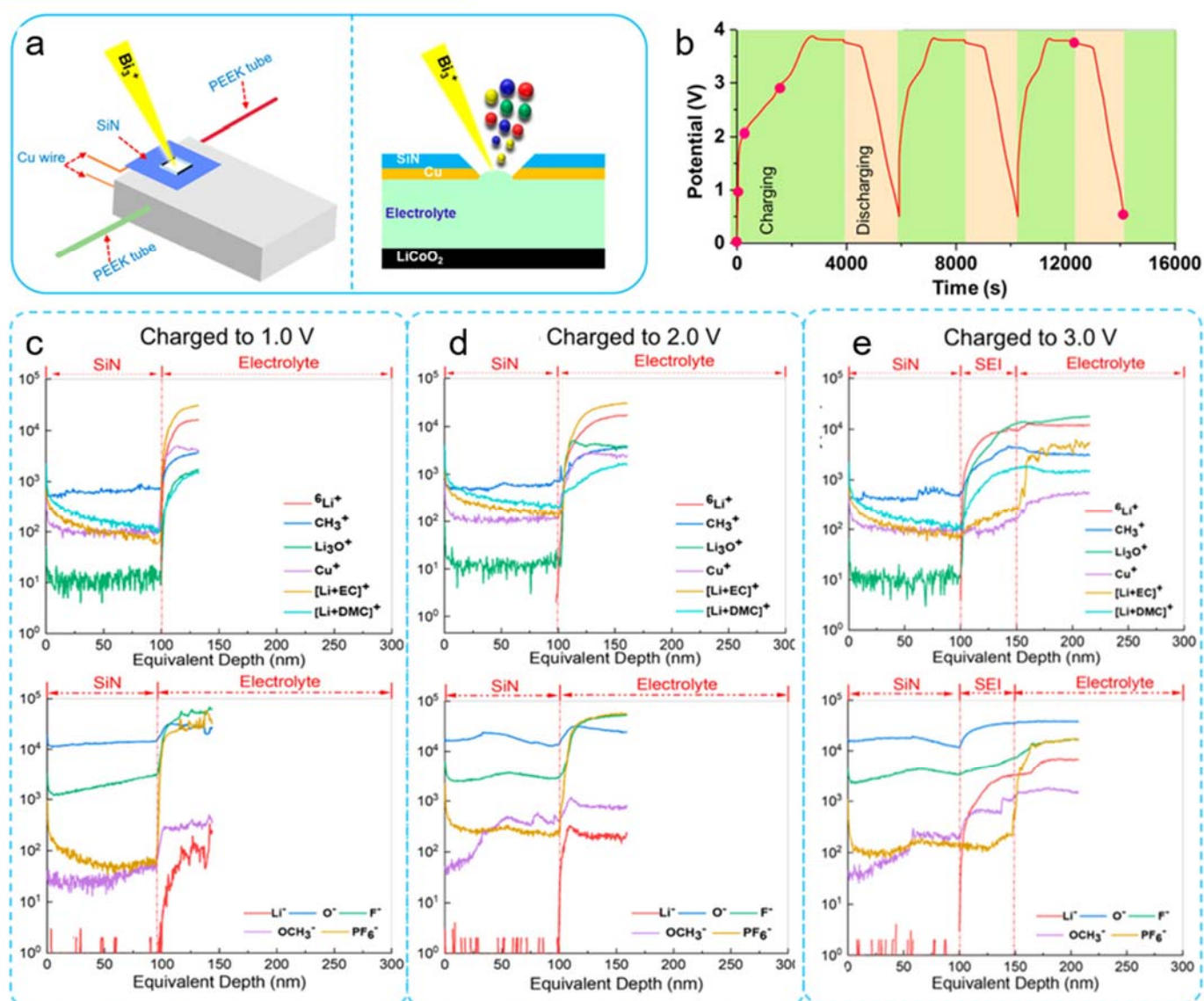
7 Recently, *operando* XPS (OXPS) was performed with a 2D-planar-like cell made of transparent glass  
 8 containing two parallel lithium foils connected to a copper current collector<sup>81</sup>. They are separated by  
 9 a cavity (0.02-0.03 cm) containing ionic liquid-based electrolyte and encapsulated in a pouch cell  
 10 configuration to fix the position of the two-lithium foil and improve the electrical contact of the cell  
 11 (Figures 11a and 11b). Here, the instrument is equipped with a micro-focused X-ray beam and a  
 12 dual beam charge neutraliser. The use of electron and ion charge neutralization guns modifies the  
 13 Fermi level of the electrode and was investigated to explore the dynamic chemical structure, as well  
 14 as the change in surface potential at the interface between lithium and electrolyte. Using IL-based  
 15 electrolytes Li/C<sub>1</sub>C<sub>6</sub>ImTFSI-LiTFSI/Li and Li/C<sub>1</sub>C<sub>6</sub>ImFSI-LiTFSI/Li, the SEI compositions were  
 16 studied by OXPS and compared with post-mortem results of coin cells by Benayard et al.<sup>81</sup>. As  
 17 shown in Figures 11c and 11d, the OXPS core level assignment (C 1s, F 1s, Li 1s, N 1s, O 1s and  
 18 S 2p) confirms the formation of LiF and the lithiated electrolyte degradation products or plated lithium  
 19 and N-heterocyclic carbenes. Although this study is still at the proof-of-concept level, this gives hope  
 20 that XPS can be applied to study the real-time dynamics of the battery electrodes and the interfaces.  
 21 Apart from the chemical component of SEI, understanding the thermal stability of SEI can be  
 22 achieved through *in situ* heating XPS. During the heating treatment, the evolution of the SEI  
 23 composition, nanostructure and the released gases can be further studied by XPS, cryo-TEM and  
 24 gas chromatography respectively, which provides deep insights for designing an ideal SEI with  
 25 enhanced stability.

26 In the future, further enhancing the temporal resolution of *operando* XPS is critical for capturing the  
 27 dynamic chemical evolution of the SEI. Developing advanced cell designs that maintain realistic  
 28 electrochemical conditions while ensuring compatibility with XPS requirements will further improve  
 29 the reliability of *operando* XPS measurements. Additionally, improving the depth-profiling capabilities  
 30 of *operando* XPS, such as through synchrotron-based techniques or angle-resolved methods, can  
 31 provide more precise insights into the spatial distribution of SEI components.

### 32 3.6 Operando Mass Spectrometry Techniques

33 The recent application of TOF-SIMs in understanding the molecular signature of the interphase  
 34 under dynamic conditions through chemical mapping of the SEI at nanometre scale<sup>82, 83</sup>. As shown

1 in Figures 12a and 12b, Cheng et al. designed a dedicated high vacuum compatible microfluidic device and used it to monitor the dynamic formation of SEI layer in Cu||LiCoO<sub>2</sub> micro-cell with 1.0 M LiPF<sub>6</sub>/EC-DMC using TOF-SIMS. Comparing the TOF-SIMS data with the fresh cell data at 1.0 V, depth profiles of the positive ions indicate the formation of an electric double layer at 1.0 V (Figure 12c) and the onset of electrolyte decomposition at 2.0 V (Figure 12d) and the formation of SEI at 3.0 V (Figure 12e). The formation of an SEI is irreversible, i.e. the SEI layer can still be observed even after discharging to 0.5 V. This means that after charging to a stable voltage of 3.8 V, it becomes difficult to penetrate the Li-enriched solid layer to expose the electrolyte. The SEI thickness is estimated to be 30-60 nm, which is consistent with the literature-reported value based on *ex situ* measurements. Additionally, the *in situ* TOF-SIMS study also confirmed that the components of electrolytes may significantly influence the thickness and homogeneity of the SEI. Future prospects include the development of highly sensitive MS systems capable of detecting trace gaseous and volatile products associated with SEI formation and decomposition in real time. Integrating *operando* MS with advanced electrochemical setups will allow simultaneous correlation of mass spectrometric data with electrochemical performance, providing deeper insights into SEI-related reactions. Innovations in isotope labelling could enhance the capability to track specific reaction pathways and identify the origins of SEI components.



18 Figure 12 (a) Schematic illustration of the microfluidic cell and the *in situ* liquid SIMS analysis of SEI. (b) Diagram of the charge-discharge process of the battery and the first three cycles (red dots represent different stages of charging and discharging). (c-e) TOF-SIMS depth profiles of representative ions measured on the interface of a Cu anode and 1.0 M LiPF<sub>6</sub>/EC-DMC electrolyte using the microcell at the fresh and different stages of charge/discharge as depicted in Figure 12b. Reproduced with permission.<sup>82</sup> Copyright 2023, ACS

1 Publications.

### 2 **3.7 Other novel techniques**

3 Molecular structural characterization techniques are crucial for understanding the composition of the  
4 SEI. For example, an ultra-thin mechanically peeled graphite was selected as the working electrode  
5 and the *in situ* setup was fabricated in a controlled argon gas environment to mitigate the influence  
6 of external factors such as water and oxygen for scanning transmission electron microscopy (STEM)  
7 study (Figures 13a and 13b). It worth noticing that, this novel *in situ* STEM technique minimized the  
8 pressure differential that develops across the Si<sub>3</sub>N<sub>4</sub> membrane windows when the fluid cell is placed  
9 in the electron microscope's high vacuum<sup>84</sup>, significantly improving the resolution and EELS signal  
10 quality. While this advanced approach offers enhanced spatial resolution and analytical capabilities,  
11 it may introduce trade-offs such as reduced liquid volume, which could limit the inventory lithium in  
12 electrolytes during the SEI formation, and increased complexity in experimental setup.

13 The electron energy loss spectroscopy (EELS) was then employed in conjunction with STEM to  
14 obtain molecule information for various constituents of the SEI layer<sup>84</sup>. These "chemical fingerprints"  
15 were subsequently applied to enable high-resolution, real-space mapping of corresponding physical  
16 structures, thus yielding nanoscale spatial resolution images depicting the SEI formation process  
17 (Figure 13c). This methodology's application served to validate previously acquired information from  
18 characterization techniques, confirming the chemically heterogeneous nature of the SEI, which  
19 primarily comprises inorganic Li compounds. Notably, no evidence indicative of a "grain boundary"  
20 akin to the typical mosaic structure of the SEI was discerned. Therefore, the authors proposed an  
21 SEI model resembling the consistency of fermenting dough, wherein distinct components do not  
22 fully mix but also do not manifest delineated boundaries.

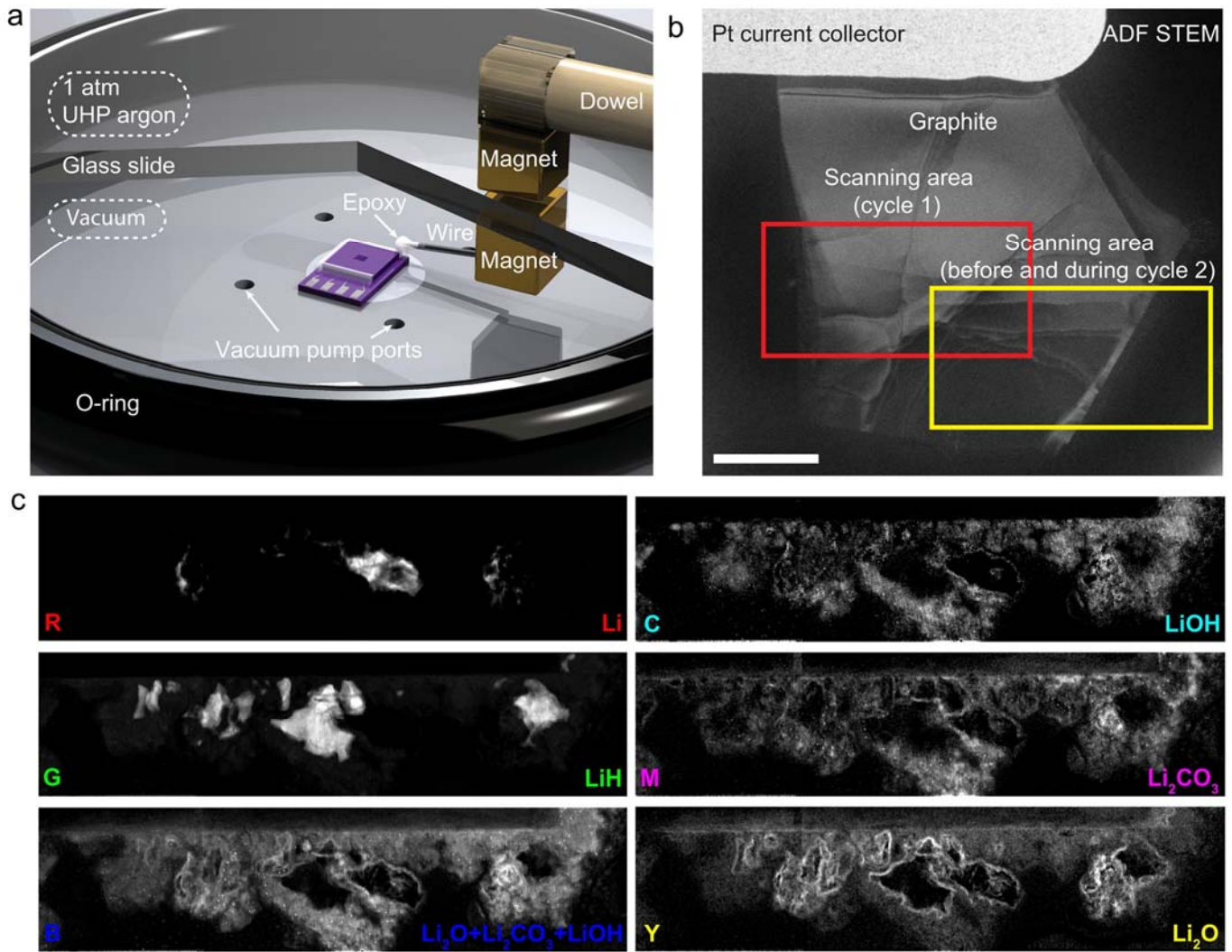


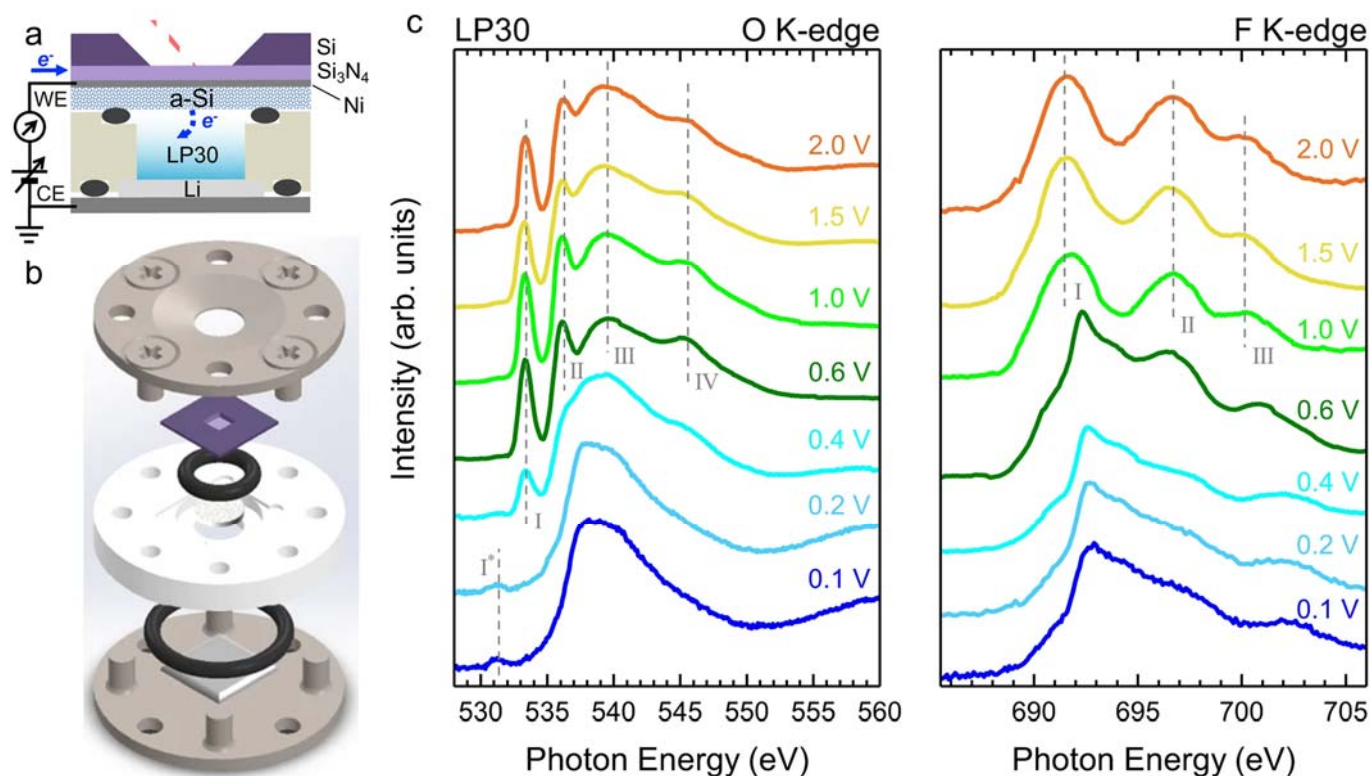
Figure 13 (a) scheme of the liquid cell imaging platform for STEM-EELS; (b) ADF STEM image of the graphite flake within a sealed fluid cell with the scale bar,  $2 \mu\text{m}$ ; (c) corresponding grayscale MLLS images with individual components of the graphite anode during cycling. Reproduced with permission. <sup>84</sup>Copyright 2023, American Association for the Advancement of Science.

Although this method provides elements and spatial chemical mapping of the SEI, it lacks information on crystal structure. Besides STEM-EELS requires more doses to obtain a decent spectrum, which is unfriendly for beam-sensitive dendrite samples. Thus, Wang et al introduced an effective four-dimensional electron microscopy analysis to reveal the spatial distribution of compounds in lithium dendrites in a large field of view. Here, the illumination beam scans across the sample and the camera records a 2D diffraction pattern at each scanning position. This results in the acquisition of a four-dimensional (4D) data set with two dimensions corresponding to real space-scanning axes and the other two dimensions representing the reciprocal axis. Hence these 4D data sets are capable of carrying abundant information about the nanostructure and its spatial distribution in the dendrite samples at low electron dose, which however not apparent and requires further extraction. A non-negative matrix factorization (NMF) algorithm was employed to decompose SEND and SCBED data sets. The SEND/SCBED-NMF scheme can provide a larger field-of-view than HRTEM and more precise composition identification with less sample damage than STEM-EELS <sup>85</sup>. Recently, Walid Dachraoui et al. employed the *operando* electrochemical liquid cell scanning transmission electron microscopy (ec-LC-STEM) to understand the structure and composition evolutions of SEI during charge/discharge cycling. The real-time observations by ADF-STEM reveal the formation of mosaic structure via two main steps as expected, ie: initial SEI nucleation where the electrolyte is reduced to form an island-like layer of LiF and then on further decomposition



1 transforms to dispersed SEI layer composed of other inorganic and organic components. This further  
2 evolves through the densification process and once the densification prevents further electrolyte  
3 decomposition, this results in an outer layer covered by organic components<sup>86</sup>.

4 Robert Whetterup and colleagues have developed an advanced *operando* soft X-ray absorption  
5 spectroscopy (sXAS) technique with nanoscale interface sensitive total electron yield mode (TEY)  
6 to monitor the crystalline, amorphous and small nanoparticles developed during the formation of the  
7 SEI layer<sup>87</sup>. This innovative approach employs a configuration reminiscent of the *in situ* liquid sXAS  
8 cell, utilizing a suspended  $\text{Si}_3\text{N}_4$  membrane, approximately 100 nm thick, acting as both an X-ray  
9 transparent and pressure-resistant window (Figures 14a and 14b). Through a meticulous analysis  
10 of O, F, and Si K-edge spectra, they revealed the temporal evolution of critical reactions taking place  
11 within the amorphous silicon anode when immersed in EC and DMC electrolytes (Figure 14c). Their  
12 findings highlighted the formation of LiF phases at ca. 0.6 V, with organic compounds, primarily  
13 composed of carbonyl groups (e.g.,  $-(\text{C}=\text{O})\text{OCH}_x$ ), emerging at potentials below 0.4 V. These results  
14 are supplemented with bulk sensitive fluorescent yield (FY) XAS measurements and density  
15 functional theory (DFT) calculated spectra. This observation is consistent with the stratified  
16 behaviour typically associated with the SEI, where LiF tends to accumulate near the anode surface,  
17 while organic components predominate in the upper layer. Additionally, the introduction of the  
18 electrolyte additive FEC was observed to enhance the generation of LiF at higher potentials,  
19 approximately 1 V. This additive played a pivotal role in passivating SEI defects, ultimately resulting  
20 in the extension of the battery's cycling lifespan. If the dynamic chemical mapping of SEI is  
21 amalgamated with this structure and component study, it will be of more significance.



#### 4. Summary and Perspectives

The formation of the SEI layer is a complex process influenced by multiple factors, and its nanoscale thickness makes it highly sensitive when exposed to air, underscoring the necessity of advanced *in*

1 *situ/operando* techniques to investigate its structural evolution and impact on battery performance.  
2 Within this review, we have outlined a series of emerging *in situ/operando* characterization  
3 techniques and summarized the newfound insights into the SEI layer garnered from the outcomes  
4 of these *in situ* tests. Nonetheless, it is paramount to acknowledge that our understanding of SEI  
5 remains far from complete. This challenge stems in part from the noticeable gap between the  
6 atomic/molecular level and the real batteries, the continual emergence of novel rechargeable battery  
7 technologies and the intricate nature of overall battery design. Consequently, we assert that  
8 forthcoming research on SEI should be directed towards reinforcing several key areas.

- 9 1. At present, *in situ* techniques primarily rely on the feedback principles from test technologies,  
10 leading to the development of *in situ* setups that are conducive for practical implementation.  
11 However, it is important to note that these techniques often exhibit a discernible disparity  
12 compared to the actual performance observed in batteries. This highlights the need for a  
13 dynamic and precise technology to monitor the growth and evolution of SEI that can be  
14 seamlessly integrated into real battery operations. Such a monitoring technique would not  
15 only facilitate an in-depth exploration of the influence exerted by various electrolyte additives  
16 and solvent compositions on SEI membranes but would also empower the rapid selection of  
17 suitable additives and electrolytes for commercial battery production. Although, the  
18 techniques cannot currently be scaled directly to large and real battery systems, it's quite  
19 feasible to extrapolate the results to larger cells through the application of AI and machine  
20 learning for predictive modelling. This, in turn, is poised to expedite the progression of battery  
21 technology, bolster battery performance, fortify reliability and safety aspects, and ultimately  
22 address the ever-growing demands within the realm of energy storage.
- 23 2. The nanoscale physical properties of the SEI layer, such as nanomechanical, thermal and  
24 electrical characteristics, are far more complex and less understood than its chemical  
25 composition, and nanostructure. At the same time, the understanding of charge transfer  
26 dynamics, porosity and the thermal stability of the SEI remains limited. Hence, gaining deeper  
27 insights into the composition-structure-property relationships of the SEI will require a detailed  
28 investigation of the physicochemical properties with a focus on the connection between its  
29 physical properties and chemical compositions. For example, the exothermic decomposition  
30 of the SEI can trigger thermal runaway in LIBs, but the thermal properties of SEI have been  
31 rarely studied<sup>88</sup>. The results from *in situ* heating XPS show that the organic components of  
32 SEI are readily decomposed even at room temperature, releasing some flammable gases  
33 (e.g., H<sub>2</sub>, CO, C<sub>2</sub>H<sub>4</sub>, etc.). The residual SEI after heat treatment is rich in inorganic  
34 components (e.g., Li<sub>2</sub>O, LiF, and Li<sub>2</sub>CO<sub>3</sub>), and provides a nanostructure model for a beneficial  
35 SEI with enhanced stability. Other techniques need to be introduced to address the  
36 knowledge gap regarding the real-time compositional evolution and gas release of SEI during  
37 heating elucidates the underlying origin for the SEI instability, and highlights its non-negligible  
38 role in regulating the thermal runaway of batteries<sup>89, 90</sup>.
- 39 3. The role of theoretical simulations is pivotal in understanding the structure and composition  
40 of the SEI.<sup>64-67</sup> Through computational analyses of SEI materials, encompassing electronic  
41 structure, lattice parameters, atomic interactions, and other fundamental attributes, an in-  
42 depth comprehension of key properties such as ion transport is attainable. Furthermore,  
43 theoretical simulations aid in the identification of potential destabilizing factors that may lead  
44 to a decline in battery performance. The outcomes of theoretical simulations enable the  
45 design and optimization of novel SEI materials, ultimately contributing to enhanced battery  
46 performance. This entails the judicious selection of material constituents, structural  
47 configurations, and additives to achieve a more stable and high-performing SEI. This  
48 approach holds substantial promise within the domains of battery material design and the  
49 augmentation of battery performance. Theoretical simulations empower the prediction of SEI

1 stability and electrochemical performance under varying material combinations, thereby  
2 facilitating the identification of the most promising SEI materials. Additionally, they will serve  
3 as a guiding framework for experimental investigations, providing a theoretical underpinning  
4 of mechanisms governing the formation and evolution of SEI.

5 4. While the trajectory of understanding the atomic/molecular level changes in real battery  
6 electrodes through *in situ/operando* characterization techniques and the macro level of the  
7 real batteries by non-invasive electrochemical characterization has seen exponential growth,  
8 there exists/remains a substantial gap ~~remains~~ between these two levels. Currently, the main  
9 process to validate the non-invasive electrochemical processing is through post-mortem  
10 characterization. Similarly, the results obtained from atomic/molecular level investigations are  
11 validated by integrating theoretical models, and simulations and projecting these results to  
12 the battery level. Although the new techniques for the non-invasive characterization of SEI in  
13 real cells is underway, the complete implementation of these methodologies alongside  
14 advanced *operando/in-situ* characterization techniques has not yet been achieved. Rather  
15 than solely projecting the atomic level/molecular level changes observed in the *operando*  
16 techniques onto real battery systems, it's crucial to integrate the non-invasive electrochemical  
17 characterization methods to better rationalize the SEI evolution and degradation modes. This  
18 bottom-up or reverse engineering approach would provide a more comprehensive  
19 understanding of SEI behaviour across different scales, helping to bridge the gap between  
20 laboratory scale insights and real-world battery performance.

21 5. The development of multi-technique coupled *in situ* characterization platforms, such as the  
22 integration of AFM with Raman spectroscopy and SECM, as well as the combination of STEM  
23 with EELS, have offered a powerful approach to acquiring diverse information about the SEI  
24 layer, including structural, compositional, and electrochemical properties, among others. This  
25 multi-technique coupled platforms with theoretical simulations offer valuable tools for  
26 addressing the complexities associated with the SEI layer. They empower researchers to  
27 delve deeper into the distribution, interactions, and alterations of different components within  
28 the SEI, thereby facilitating a more profound understanding of its formation mechanisms and  
29 properties. We believed further integrating various non-invasive characterization techniques  
30 could enable a more precise description of SEI properties and a better comprehension of  
31 their correlation with battery performance. The development of such platforms not only  
32 deepens our understanding of SEI behaviour but also holds significant potential for advancing  
33 battery research and enhancing overall performance and safety.

34 Overall, a more comprehensive understanding of SEI structure-composition-property correlations  
35 informed by these advanced techniques not only addresses current characterization challenges in  
36 battery technology, but also supports the SEI optimization and revolutionize battery design. By  
37 elucidating the structural, chemical, and electrochemical properties of the SEI layer, researchers  
38 can identify key factors that influence its stability, ionic conductivity, and mechanical integrity. These  
39 insights pave the way for tailoring electrolyte compositions and additives that promote the formation  
40 of a thin, robust, homogeneous SEI with minimal side reactions, which are critical for improving  
41 battery safety and extending cycle life.

## 42 Acknowledgements

43 H.L.<sup>1</sup> and N.M.<sup>1</sup> contribute equality to this perspective. The authors acknowledge the financial  
44 support by the National Natural Science Foundation of China (No. 62474041 and 52403294), the  
45 Faraday Institution (grant number FIRG018), EPSRC project EP/V00767X/1, and the Science  
46 Foundation of the Fujian Province (2023J01521).

## 47 References

1. Peljo, P.; Girault, H. H., Electrochemical potential window of battery electrolytes: the HOMO-LUMO misconception. *Energ Environ Sci* **2018**, *11* (9), 2306-2309.
2. Goodenough, J. B.; Kim, Y., Challenges for Rechargeable Li Batteries. *Chem Mater* **2010**, *22* (3), 587-603.
3. Peled, E.; Menkin, S., Review-SEI: Past, Present and Future. *J Electrochem Soc* **2017**, *164* (7), A1703-A1719.
4. Adenusi, H.; Chass, G. A.; Passerini, S.; Tian, K. V.; Chen, G., Lithium Batteries and the Solid Electrolyte Interphase (SEI)—Progress and Outlook. **2023**, *13* (10), 2203307.
5. Tan, J.; Matz, J.; Dong, P.; Shen, J.; Ye, M., A Growing Appreciation for the Role of LiF in the Solid Electrolyte Interphase. **2021**, *11* (16), 2100046.
6. Yan, C.; Xu, R.; Xiao, Y.; Ding, J.-F.; Xu, L.; Li, B.-Q.; Huang, J.-Q., Toward Critical Electrode/Electrolyte Interfaces in Rechargeable Batteries. *Advanced Functional Materials* **2020**, *30* (23), 1909887.
7. Feng, X.; Ren, D.; He, X.; Ouyang, M., Mitigating Thermal Runaway of Lithium-Ion Batteries. *Joule* **2020**, *4* (4), 743-770.
8. Li, B.; Chao, Y.; Li, M.; Xiao, Y.; Li, R.; Yang, K.; Cui, X.; Xu, G.; Li, L.; Yang, C.; Yu, Y.; Wilkinson, D. P.; Zhang, J., A Review of Solid Electrolyte Interphase (SEI) and Dendrite Formation in Lithium Batteries. *Electrochemical Energy Reviews* **2023**, *6* (1), 7.
9. Wan, H.; Xu, J.; Wang, C., Designing electrolytes and interphases for high-energy lithium batteries. *Nature Reviews Chemistry* **2024**, *8* (1), 30-44.
10. Asfaw, H. D.; Kotronia, A.; Garcia-Araez, N.; Edström, K.; Brandell, D., Charting the course to solid-state dual-ion batteries. **2024**, *6* (3), e425.
11. Chen, Y.; Wu, W. K.; Gonzalez-Munoz, S.; Forcieri, L.; Wells, C.; Jarvis, S. P.; Wu, F. L.; Young, R.; Dey, A.; Isaacs, M.; Nagarathinam, M.; Palgrave, R. G.; Tapia-Ruiz, N.; Kolosov, O. V., Nanoarchitecture factors of solid electrolyte interphase formation via 3D nano-rheology microscopy and surface force-distance spectroscopy. *Nature Communications* **2023**, *14* (1).
12. Kyeremateng, N. A.; Elia, G. A.; Hahn, R.; Slater, P. R., Lithium-Ion Batteries: Nomenclature of Interphases with Liquid or Solid-State Electrolytes. *Batteries & Supercaps* **2023**, *6* (3).
13. Shan, X. Y.; Zhong, Y.; Zhang, L. J.; Zhang, Y. Q.; Xia, X. H.; Wang, X. L.; Tu, J. P., A Brief Review on Solid Electrolyte Interphase Composition Characterization Technology for Lithium Metal Batteries: Challenges and Perspectives. *J Phys Chem C* **2021**, *125* (35), 19060-19080.
14. Cheng, X. B.; Zhang, R.; Zhao, C. Z.; Wei, F.; Zhang, J. G.; Zhang, Q., A Review of Solid Electrolyte Interphases on Lithium Metal Anode. *Adv Sci (Weinh)* **2016**, *3* (3), 1500213.
15. Villevieille, C., Interfaces and Interphases in Batteries: How to Identify and Monitor Them Properly Using Surface Sensitive Characterization Techniques. *Adv Mater Interfaces* **2022**, *9* (8), 2101865.
16. Xu, K., Interfaces and interphases in batteries. *J Power Sources* **2023**, 559.
17. Peled, E.; Golodnitsky, D.; Ardel, G., Advanced model for solid electrolyte interphase electrodes in liquid and polymer electrolytes. *J Electrochem Soc* **1997**, *144* (8), L208-L210.
18. Aurbach, D., Review of selected electrode-solution interactions which determine the performance of Li and Li ion batteries. *J Power Sources* **2000**, *89* (2), 206-218.
19. Li, Y. Z.; Li, Y. B.; Pei, A. L.; Yan, K.; Sun, Y. M.; Wu, C. L.; Joubert, L. M.; Chin, R.; Koh, A. L.; Yu, Y.; Perrino, J.; Butz, B.; Chu, S.; Cui, Y., Atomic structure of sensitive battery materials and Interfaces revealed by cryo-electron microscopy. *Science* **2017**, *358* (6362), 506-510.
20. Liu, P.; Shen, S.; Qiu, Z.; Yang, T.; Liu, Y.; Su, H.; Zhang, Y.; Li, J.; Cao, F.; Zhong, Y.; Liang, X.; Chen, M.; He, X.; Xia, Y.; Wang, C.; Wan, W.; Tu, J.; Zhang, W.; Xia, X., Plasma Coupled Electrolyte Additive Strategy for Construction of High-Performance Solid Electrolyte Interphase on Li Metal Anodes. **2024**, *36* (30), 2312812.
21. Menkin, S.; O'Keefe, C. A.; Gunnarsdóttir, A. B.; Dey, S.; Pesci, F. M.; Shen, Z. H.; Aguadero, A.; Grey, C. P., Toward an Understanding of SEI Formation and Lithium Plating on Copper in Anode-Free Batteries. *J Phys Chem C* **2021**, *125* (30), 16719-16732.
22. Tripathi, A. M.; Su, W. N.; Hwang, B. J., In situ analytical techniques for battery interface analysis. *Chem Soc Rev* **2018**, *47* (3), 736-851.

23. Wu, J.; Ihsan-Ul-Haq, M.; Chen, Y.; Kim, J.-K., Understanding solid electrolyte interphases: Advanced characterization techniques and theoretical simulations. *Nano Energy* **2021**, *89*.
24. Zhang, Z. Y.; Said, S.; Smith, K.; Jervis, R.; Howard, C. A.; Shearing, P. R.; Brett, D. J. L.; Miller, T. S., Characterizing Batteries by In Situ Electrochemical Atomic Force Microscopy: A Critical Review. *Advanced Energy Materials* **2021**, *11* (38).
25. Wang, A. P.; Kadam, S.; Li, H.; Shi, S. Q.; Qi, Y., Review on modeling of the anode solid electrolyte interphase (SEI) for lithium-ion batteries. *Npj Computational Materials* **2018**, *4*.
26. Pérez-Villar, S.; Lanz, P.; Schneider, H.; Novák, P., Characterization of a model solid electrolyte interphase/carbon interface by combined Raman/Fourier transform infrared microscopy. *Electrochim Acta* **2013**, *106*, 506-515.
27. Xu, Y. L.; Dong, K.; Jie, Y. L.; Adelhelm, P.; Chen, Y. W.; Xu, L.; Yu, P. P.; Kim, J.; Kochovski, Z.; Yu, Z. L.; Li, W. X.; LeBeau, J.; Shao-Horn, Y.; Cao, R. G.; Jiao, S. H.; Cheng, T.; Manke, I.; Lu, Y., Promoting Mechanistic Understanding of Lithium Deposition and Solid-Electrolyte Interphase (SEI) Formation Using Advanced Characterization and Simulation Methods: Recent Progress, Limitations, and Future Perspectives. *Advanced Energy Materials* **2022**, *12* (19).
28. Xu, C.; Lindgren, F.; Philippe, B.; Gorgoi, M.; Björefors, F.; Edström, K.; Gustafsson, T., Improved Performance of the Silicon Anode for Li-Ion Batteries: Understanding the Surface Modification Mechanism of Fluoroethylene Carbonate as an Effective Electrolyte Additive. *Chem Mater* **2015**, *27* (7), 2591-2599.
29. Aurbach, D.; Weissman, I.; Schechter, A.; Cohen, H., X-ray photoelectron spectroscopy studies of lithium surfaces prepared in several important electrolyte solutions. A comparison with previous studies by Fourier transform infrared spectroscopy. *Langmuir* **1996**, *12* (16), 3991-4007.
30. Hope, M. A.; Rinkel, B. L. D.; Gunnarsdóttir, A. B.; Märker, K.; Menkin, S.; Paul, S.; Sergeyev, I. V.; Grey, C. P., Selective NMR observation of the SEI-metal interface by dynamic nuclear polarisation from lithium metal. *Nature communications* **2020**, *11* (1), 2224.
31. Zhang, Z. W.; Li, Y. Z.; Xu, R.; Zhou, W. J.; Li, Y. B.; Oyakhire, S. T.; Wu, Y. C.; Xu, J. W.; Wang, H. S.; Yu, Z. A.; Boyle, D. T.; Huang, W.; Ye, Y. S.; Chen, H.; Wan, J. Y.; Bao, Z. N.; Chiu, W.; Cui, Y., Capturing the swelling of solid-electrolyte interphase in lithium metal batteries. *Science* **2022**, *375* (6576), 66-+.
32. He, Y.; Jiang, L.; Chen, T. W.; Xu, Y. B.; Jia, H. P.; Yi, R.; Xue, D. C.; Song, M.; Genc, A.; Bouchet-Marquis, C.; Pullan, L.; Tessner, T.; Yoo, J.; Li, X. L.; Zhang, J. G.; Zhang, S. L.; Wang, C. M., Progressive growth of the solid-electrolyte interphase towards the Si anode interior causes capacity fading. *Nature Nanotechnology* **2021**, *16* (10), 1113-+.
33. Han, B.; Zhang, Z.; Zou, Y. C.; Xu, K.; Xu, G. Y.; Wang, H.; Meng, H.; Deng, Y. H.; Li, J.; Gu, M., Poor Stability of LiCO in the Solid Electrolyte Interphase of a Lithium-Metal Anode Revealed by Cryo-Electron Microscopy. *Adv Mater* **2021**, *33* (22).
34. Li, Y. Z.; Huang, W.; Li, Y. B.; Pei, A.; Boyle, D. T.; Cui, Y., Correlating Structure and Function of Battery Interphases at Atomic Resolution Using Cryoelectron Microscopy. *Joule* **2018**, *2* (10), 2167-2177.
35. Das Goswami, B. R.; Jabbari, V.; Shahbazian-Yassar, R.; Mashayek, F.; Yurkiv, V., Unraveling Ion Diffusion Pathways and Energetics in Polycrystalline SEI of Lithium-Based Batteries: Combined Cryo-HRTEM and DFT Study. *J Phys Chem C* **2023**, *127* (45), 21971-21979.
36. Hui, J. S.; Gossage, Z. T.; Sarbapalli, D.; Hernández-Burgos, K.; Rodríguez-López, J., Advanced Electrochemical Analysis for Energy Storage Interfaces. *Analytical Chemistry* **2019**, *91* (1), 60-83.
37. Chen, Y.; Pan, H. D. A.; Lin, C.; Li, J. X.; Cai, R. S.; Haigh, S. J.; Zhao, G. Y.; Zhang, J. M.; Lin, Y. B.; Kolosov, O. V.; Huang, Z. G., Controlling Interfacial Reduction Kinetics and Suppressing Electrochemical Oscillations in LiTiO Thin-Film Anodes. *Advanced Functional Materials* **2021**, *31* (43).
38. Zhou, S.; Panse, K. S.; Motevaselian, M. H.; Aluru, N. R.; Zhang, Y. J., Three-Dimensional Molecular Mapping of Ionic Liquids at Electrified Interfaces. *Acs Nano* **2020**, *14* (12), 17515-17523.
39. Uhlig, M. R.; Garcia, R., Atomic-Scale Imaging of Interfacial Water under 3D Nanoscale Confinement. *Nano Lett* **2021**, *21* (13), 5593-5598.

40. Black, J. M.; Walters, D.; Labuda, A.; Feng, G.; Hillesheim, P. C.; Dai, S.; Cummings, P. T.; Kalinin, S. V.; Proksch, R.; Balke, N., Bias-Dependent Molecular-Level Structure of Electrical Double Layer in Ionic Liquid on Graphite. *Nano Lett* **2013**, *13* (12), 5954-5960.
41. Zhang, W. L.; Lu, Y.; Wan, L.; Zhou, P.; Xia, Y. C.; Yan, S. S.; Chen, X. X.; Zhou, H. Y.; Dong, H.; Liu, K., Engineering a passivating electric double layer for high performance lithium metal batteries. *Nature Communications* **2022**, *13* (1).
42. Benaglia, S.; Uhlig, M. R.; Hernández-Muñoz, J.; Chacón, E.; Tarazona, P.; Garcia, R., Tip Charge Dependence of Three-Dimensional AFM Mapping of Concentrated Ionic Solutions. *Phys Rev Lett* **2021**, *127* (19).
43. Gossage, Z. T.; Hui, J. S.; Zeng, Y. X.; Flores-Zuleta, H.; Rodríguez-López, J., Probing the reversibility and kinetics of Li during SEI formation and (de)intercalation on edge plane graphite using ion-sensitive scanning electrochemical microscopy. *Chemical Science* **2019**, *10* (46), 10749-10754.
44. Martín-Yerga, D.; Kang, M.; Unwin, P. R., Scanning Electrochemical Cell Microscopy in a Glovebox: Structure-Activity Correlations in the Early Stages of Solid-Electrolyte Interphase Formation on Graphite. *Chemelectrochem* **2021**, *8* (22), 4240-4251.
45. Polcari, D.; Dauphin-Ducharme, P.; Mauzeroll, J., Scanning Electrochemical Microscopy: A Comprehensive Review of Experimental Parameters from 1989 to 2015. *Chem Rev* **2016**, *116* (22), 13234-13278.
46. Mefford, J. T.; Akbashev, A. R.; Kang, M. K.; Bentley, C. L.; Gent, W. E.; Deng, H. T. D.; Alsem, D. H.; Yu, Y. S.; Salmon, N. J.; Shapiro, D. A.; Unwin, P. R.; Chueh, W. C., Correlative operando microscopy of oxygen evolution electrocatalysts. *Nature* **2021**, *593* (7857), 67-+.
47. Krumov, M. R.; Lang, S. Y.; Johnson, L.; Abruna, H. D., Operando Investigation of Solid Electrolyte Interphase Formation, Dynamic Evolution, and Degradation During Lithium Plating/Stripping. *Acs Appl Mater Inter* **2023**, *15* (40), 47692-47703.
48. Wahab, O. J.; Daviddi, E.; Xin, B.; Sun, P. Z.; Griffin, E.; Colburn, A. W.; Barry, D.; Yagmurcukardes, M.; Peeters, F. M.; Geim, A. K.; Lozada-Hidalgo, M.; Unwin, P. R., Proton transport through nanoscale corrugations in two-dimensional crystals. *Nature* **2023**, *620* (7975).
49. Xue, Y. B.; Jia, H.; Gao, P. Y.; Galvez-Aranda, D. E.; Beltran, S. P.; Cao, X.; Le, P. M. L.; Liu, J. F.; Engelhard, M. H.; Li, S.; Ren, G.; Seminario, J. M.; Balbuena, P. B.; Zhang, J. G.; Xu, W.; Wang, C. M., Direct in situ measurements of electrical properties of solid-electrolyte interphase on lithium metal anodes. *Nat Energy* **2023**, *8* (11), 1345-1354.
50. Krauss, F. T.; Pantenburg, I.; Roling, B., Transport of Ions, Molecules, and Electrons across the Solid Electrolyte Interphase: What Is Our Current Level of Understanding? *Adv Mater Interfaces* **2022**, *9* (8).
51. Gu, Y.; You, E. M.; Lin, J. D.; Wang, J. H.; Luo, S. H.; Zhou, R. Y.; Zhang, C. J.; Yao, J. L.; Li, H. Y.; Li, G.; Wang, W. W.; Qiao, Y.; Yan, J. W.; Wu, D. Y.; Liu, G. K.; Zhang, L.; Li, J. F.; Xu, R.; Tian, Z. Q.; Cui, Y.; Mao, B. W., Resolving nanostructure and chemistry of solid-electrolyte interphase on lithium anodes by depth-sensitive plasmon-enhanced Raman spectroscopy. *Nature Communications* **2023**, *14* (1).
52. Lu, X. K.; Lagnoni, M.; Bertei, A.; Das, S.; Owen, R. E.; Li, Q.; O'Regan, K.; Wade, A.; Finegan, D. P.; Kendrick, E.; Bazant, M. Z.; Brett, D. J. L.; Shearing, P. R., Multiscale dynamics of charging and plating in graphite electrodes coupling operando microscopy and phase-field modelling. *Nature Communications* **2023**, *14* (1).
53. Merryweather, A. J.; Jacquet, Q.; Emge, S. P.; Schnedermann, C.; Rao, A.; Grey, C. P., Operando monitoring of single-particle kinetic state-of-charge heterogeneities and cracking in high-rate Li-ion anodes. *Nat Mater* **2022**, *21* (11), 1306-+.
54. Pandya, R.; Valzania, L.; Dorchie, F.; Xia, F.; Mc Hugh, J.; Mathieson, A.; Tan, H. J.; Parton, T. G.; Godeffroy, L.; Mazloomian, K.; Miller, T. S.; Kanoufi, F.; De Volder, M.; Tarascon, J. M.; Gigan, S.; de Aguiar, H. B.; Grimaud, A., Three-dimensional operando optical imaging of particle and electrolyte heterogeneities inside Li-ion batteries. *Nature Nanotechnology* **2023**, *18* (10), 1185-+.
55. Feng, G. X.; Jia, H.; Shi, Y. P.; Yang, X.; Liang, Y. L.; Engelhard, M. H.; Zhang, Y.; Yang,

- 1 C. J.; Xu, K.; Yao, Y.; Xu, W.; Shan, X. A., Imaging solid-electrolyte interphase dynamics using  
2 operando reflection interference microscopy. *Nature Nanotechnology* **2023**, *18* (7), 780-+.
- 3 56. Merryweather, A. J.; Schnedermann, C.; Jacquet, Q.; Grey, C. P.; Rao, A. K., Operando  
4 optical tracking of single-particle ion dynamics in batteries. *Nature* **2021**, *594* (7864), 522-+.
- 5 57. Gajan, A.; Lecourt, C.; Bautista, B. E. T.; Fillaud, L.; Demeaux, J.; Lucas, I. T., Solid  
6 Electrolyte Interphase Instability in Operating Lithium-Ion Batteries Unraveled by Enhanced-Raman  
7 Spectroscopy. *Acs Energy Lett* **2021**, *6* (5), 1757-1763.
- 8 58. Chen, Y.; Zhang, S.; Ye, J.; Zheng, X.; Zhang, J.-M.; Mangayarkarasi, N.; Niu, Y.; Lu, H.;  
9 Zhao, G.; Tao, J.; Li, J.; Lin, Y.; Kolosov, O. V.; Huang, Z., Nonequilibrium fast-lithiation of  
10 Li<sub>4</sub>Ti<sub>5</sub>O<sub>12</sub> thin film anode for LIBs. *Communications Physics* **2024**, *7* (1), 280.
- 11 59. Shi, Y. P.; Feng, G. X.; Li, X. L.; Yang, X.; Ghanim, A. H.; Ruchhoeft, P.; Jackson, D.;  
12 Mubeen, S.; Shan, X. N., Electrochemical Impedance Imaging on Conductive Surfaces. *Analytical*  
13 *Chemistry* **2021**, *93* (36), 12320-12328.
- 14 60. Dopilka, A.; Gu, Y. R.; Larson, J. M.; Zorba, V.; Kostecky, R., Nano-FTIR Spectroscopy of  
15 the Solid Electrolyte Interphase Layer on a Thin-Film Silicon Li-Ion Anode. *Acs Appl Mater Inter*  
16 **2023**.
- 17 61. Imhof, R.; Novak, P., In situ investigation of the electrochemical reduction of carbonate  
18 electrolyte solutions at graphite electrodes. *J Electrochem Soc* **1998**, *145* (4), 1081-1087.
- 19 62. Hy, S.; Felix; Chen, Y. H.; Liu, J. Y.; Rick, J.; Hwang, B. J., surface enhanced Raman  
20 spectroscopic studies of solid electrolyte interphase formation in lithium ion battery electrodes. *J*  
21 *Power Sources* **2014**, *256*, 324-328.
- 22 63. Gogoi, N.; Melin, T.; Berg, E. J., Elucidating the Step-Wise Solid Electrolyte Interphase  
23 Formation in Lithium-Ion Batteries with Operando Raman Spectroscopy. *Adv Mater Interfaces* **2022**,  
24 *9* (22).
- 25 64. Narayanan, A.; Mugele, F.; Duits, M. H. G., Electrochemically Induced Changes in TiO  
26 and Carbon Films Studied with QCM-D. *Acs Applied Energy Materials* **2020**, *3* (2), 1775-1783.
- 27 65. Levi, M. D.; Daikhin, L.; Aurbach, D.; Presser, V., Quartz Crystal Microbalance with  
28 Dissipation Monitoring (EQCM-D) for in-situ studies of electrodes for supercapacitors and batteries:  
29 A mini-review. *Electrochem Commun* **2016**, *67*, 16-21.
- 30 66. Dargel, V.; Shpigel, N.; Sigalov, S.; Nayak, P.; Levis, M. D.; Daikhin, L.; Aurbach, D., In  
31 situ real-time gravimetric and viscoelastic probing of surface films formation on lithium batteries  
32 electrodes. *Nature Communications* **2017**, *8*.
- 33 67. Sayavong, P.; Zhang, W. B.; Oyakhire, S. T.; Boyle, D. T.; Chen, Y. L.; Kim, S. C.; Vilá, R.;  
34 Holmes, S. E.; Kim, M. S.; Bent, S. F.; Bao, Z. A.; Cui, Y., Dissolution of the Solid Electrolyte  
35 Interphase and Its Effects on Lithium Metal Anode Cyclability. *Journal of the American Chemical*  
36 *Society* **2023**, *145* (22), 12342-12350.
- 37 68. Bendadesse, E.; Morozov, A. V.; Abakumov, A. M.; Perrot, H.; Tarascon, J. M.; Sel, O.,  
38 Deciphering the Double-Layer Structure and Dynamics on a Model Li
- 39 MoO
- 40 Interface by Advanced Electrogravimetric Analysis. *Acs Nano* **2022**, *16* (9), 14907-14917.
- 41 69. Mozhzhukhina, N.; Flores, E.; Lundström, R.; Nyström, V.; Kitz, P. G.; Edström, K.; Berg,  
42 E. J., Direct Observation of Double Layer Charging and Early Solid Electrolyte Interphase Formation  
43 in Li-Ion Battery Electrolytes. *J Phys Chem Lett* **2020**, *11* (10), 4119-4123.
- 44 70. Yang, Z. Z.; Leon, N. J.; Liao, C.; Ingram, B. J.; Trahey, L., Effect of Salt Concentration on  
45 the Interfacial Solvation Structure and Early Stage of Solid-Electrolyte Interphase Formation in  
46 Ca(BH)/THF for Ca Batteries. *Acs Appl Mater Inter* **2023**, *15* (20), 25018-25028.
- 47 71. Kwon, B.; Lee, J.; Kim, H.; Kim, D. M.; Park, K.; Jo, S.; Lee, K. T., Janus behaviour of  
48 LiFSI- and LiPF
- 49 -based electrolytes for Li metal batteries: chemical corrosion
- 50 galvanic corrosion. *J Mater Chem A* **2021**, *9* (44), 24993-25003.

72. Lei, W.; Li, H.; Tang, Y.; Shao, H., Progress and perspectives on electrospinning techniques for solid-state lithium batteries. **2022**, 4 (4), 539-575.
73. Liu, P.; Qiu, Z.; Cao, F.; Zhang, Y.; He, X.; Shen, S.; Liang, X.; Chen, M.; Wang, C.; Wan, W.; Xia, Y.; Xia, X.; Zhang, W., Liquid-source plasma technology for construction of dual bromine-fluorine-enriched interphases on lithium metal anodes with enhanced performance. *Journal of Materials Science & Technology* **2024**, 177, 68-78.
74. Scivetti, I.; Teobaldi, G., ALC\_EQCM: Automated stoichiometric resolution in electrochemistry through Density Functional Theory aided, Electrochemical Quartz Crystal Microbalance. *Comp Mater Sci* **2023**, 218.
75. Moeremans, B.; Cheng, H. W.; Merola, C.; Hu, Q. Y.; Oezaslan, M.; Safari, M.; Van Bael, M. K.; Hardy, A.; Valtiner, M.; Renner, F. U., In Situ Mechanical Analysis of the Nanoscopic Solid Electrolyte Interphase on Anodes of Li-Ion Batteries. *Adv Sci* **2019**, 6 (16).
76. Moeremans, B.; Cheng, H. W.; Hu, Q. Y.; Garces, H. F.; Padture, N. P.; Renner, F. U.; Valtiner, M., Lithium-ion battery electrolyte mobility at nano-confined graphene interfaces. *Nature Communications* **2016**, 7.
77. Källquist, I.; Le Ruyet, R.; Liu, H.; Mogensen, R.; Lee, M.-T.; Edström, K.; Naylor, A. J., Advances in studying interfacial reactions in rechargeable batteries by photoelectron spectroscopy. *J Mater Chem A* **2022**, 10 (37), 19466-19505.
78. Ogletree, D. F.; Bluhm, H.; Lebedev, G.; Fadley, C. S.; Hussain, Z.; Salmeron, M., A differentially pumped electrostatic lens system for photoemission studies in the millibar range. *Rev Sci Instrum* **2002**, 73 (11), 3872-3877.
79. Kallquist, I.; Lindgren, F.; Lee, M. T.; Shavorskiy, A.; Edstrom, K.; Rensmo, H.; Nyholm, L.; Maibach, J.; Hahlin, M., Probing Electrochemical Potential Differences over the Solid/Liquid Interface in Li-Ion Battery Model Systems. *ACS Appl Mater Interfaces* **2021**, 13 (28), 32989-32996.
80. Dietrich, P.; Gehrlein, L.; Maibach, J.; Thissen, A., Probing Lithium-Ion Battery Electrolytes with Laboratory Near-Ambient Pressure XPS. *Crystals* **2020**, 10 (11).
81. Benayad, A.; Morales-Ugarte, J. E.; Santini, C. C.; Bouchet, R., Operando XPS: A Novel Approach for Probing the Lithium/Electrolyte Interphase Dynamic Evolution. *J Phys Chem A* **2021**, 125 (4), 1069-1081.
82. Cheng, C. X.; Zhou, Y. D.; Xu, Y. B.; Jia, H.; Kim, J.; Xu, W.; Wang, C. M.; Gao, P. Y.; Zhu, Z. H., Dynamic Molecular Investigation of the Solid-Electrolyte Interphase of an Anode-Free Lithium Metal Battery Using Liquid SIMS and Cryo-TEM. *Nano Lett* **2023**, 23 (18), 8385-8391.
83. Zhou, Y.; Su, M.; Yu, X.; Zhang, Y.; Wang, J.-G.; Ren, X.; Cao, R.; Xu, W.; Baer, D. R.; Du, Y.; Borodin, O.; Wang, Y.; Wang, X.-L.; Xu, K.; Xu, Z.; Wang, C.; Zhu, Z., Real-time mass spectrometric characterization of the solid–electrolyte interphase of a lithium-ion battery. *Nature nanotechnology* **2020**, 15 (3), 224-230.
84. Lodico, J. J.; Mecklenburg, M.; Chan, H. L.; Chen, Y. Y.; Ling, X. Y.; Regan, B. C., Operando spectral imaging of the lithium ion battery's solid-electrolyte interphase. *Sci Adv* **2023**, 9 (28).
85. Wang, Z. Y.; Zhai, W. B.; Yu, Y., Revealing the Distribution of Lithium Compounds in Lithium Dendrites by Four-Dimensional Electron Microscopy Analysis. *Nano Lett* **2024**, 24 (8), 2537-2543.
86. Dachraoui, W.; Pauer, R.; Battaglia, C.; Erni, R., Operando Electrochemical Liquid Cell Scanning Transmission Electron Microscopy Investigation of the Growth and Evolution of the Mosaic Solid Electrolyte Interphase for Lithium-Ion Batteries. *ACS nano* **2023**, 17 (20), 20434-20444.
87. Swallow, J. E. N.; Fraser, M. W.; Kneusels, N. H.; Charlton, J. F.; Sole, C. G.; Phelan, C. M. E.; Bjorklund, E.; Bencok, P.; Escudero, C.; Perez-Dieste, V.; Grey, C. P.; Nicholls, R. J.; Weatherup, R. S., Revealing solid electrolyte interphase formation through interface-sensitive Operando X-ray absorption spectroscopy. *Nat Commun* **2022**, 13 (1), 6070.
88. Huang, S.; Cheong, L.-Z.; Wang, D.; Shen, C., Thermal stability of solid electrolyte interphase of lithium-ion batteries. *Appl. Surf. Sci.* **2018**, 454, 61-67.
89. Wu, J. P.; Weng, S. T.; Zhang, X.; Sun, W. W.; Wu, W.; Wang, Q. Y.; Yu, X. Q.; Chen, L. Q.; Wang, Z. X.; Wang, X. F., In Situ Detecting Thermal Stability of Solid Electrolyte Interphase (SEI). *Small* **2023**, 19 (25).



1 90. Yoon, T.; Millen, M. S.; Parimalam, B. S.; Lucht, B. L., Thermal Decomposition of the Solid  
2 Electrolyte Interphase (SEI) on Silicon Electrodes for Lithium Ion Batteries. *Chem Mater* **2017**, *29*  
3 (7), 3237-3245.

4